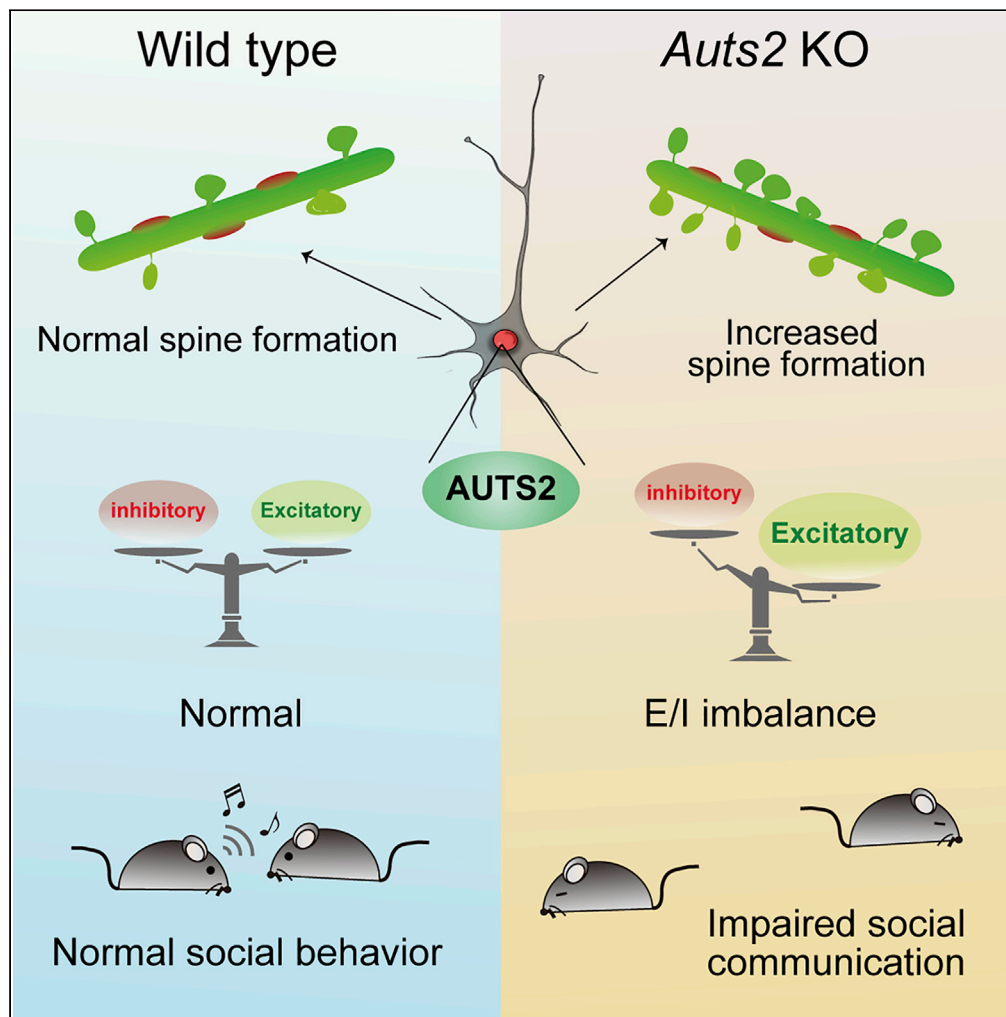


Article

AUTS2 Regulation of Synapses for Proper Synaptic Inputs and Social Communication



Kei Hori, Kunihiko Yamashiro, Taku Nagai, ..., Mitsuhiro Yamada, Kiyofumi Yamada, Mikio Hoshino

khori@ncnp.go.jp (K.H.)
hoshino@ncnp.go.jp (M.H.)

HIGHLIGHTS

AUTS2 regulates excitatory synapse number in forebrain pyramidal neurons

Loss of *Auts2* leads to increased spine formation in development and adulthood

Loss of *Auts2* alters the balance of excitatory and inhibitory synaptic inputs

Auts2 mutant mice exhibit cognitive and sociobehavioral deficits

Hori et al., iScience 23, 101183
June 26, 2020 © 2020 The Authors.
<https://doi.org/10.1016/j.isci.2020.101183>



Article

AUTS2 Regulation of Synapses for Proper Synaptic Inputs and Social Communication

Kei Hori,^{1,*} Kunihiko Yamashiro,¹ Taku Nagai,² Wei Shan,² Saki F. Egusa,¹ Kazumi Shimaoka,¹ Hiroshi Kuniishi,^{3,4} Masayuki Sekiguchi,⁴ Yasuhiro Go,^{5,6,7} Shoji Tatsumoto,⁵ Mitsuyo Yamada,^{1,8} Reika Shiraishi,¹ Kouta Kanno,⁹ Satoshi Miyashita,¹ Asami Sakamoto,¹ Manabu Abe,^{10,12} Kenji Sakimura,^{10,12} Masaki Sone,⁸ Kazuhiro Sohya,¹¹ Hiroshi Kunugi,¹¹ Keiji Wada,⁴ Mitsuhiro Yamada,³ Kiyofumi Yamada,² and Mikio Hoshino^{1,13,*}

SUMMARY

Impairments in synapse development are thought to cause numerous psychiatric disorders. Autism susceptibility candidate 2 (AUTS2) gene has been associated with various psychiatric disorders, such as autism and intellectual disabilities. Although roles for AUTS2 in neuronal migration and neuritogenesis have been reported, its involvement in synapse regulation remains unclear. In this study, we found that excitatory synapses were specifically increased in the *Auts2*-deficient primary cultured neurons as well as *Auts2* mutant forebrains. Electrophysiological recordings and immunostaining showed increases in excitatory synaptic inputs as well as *c-fos* expression in *Auts2* mutant brains, suggesting that an altered balance of excitatory and inhibitory inputs enhances brain excitability. *Auts2* mutant mice exhibited autistic-like behaviors including impairments in social interaction and altered vocal communication. Together, these findings suggest that AUTS2 regulates excitatory synapse number to coordinate E/I balance in the brain, whose impairment may underlie the pathology of psychiatric disorders in individuals with AUTS2 mutations.

INTRODUCTION

Synapses form the basis for the neuronal network and brain function. Development of synapses, synaptogenesis, is precisely regulated by genetic programs as well as synaptic activities. Even after establishment of the fundamental brain structures, synapses are dynamically formed and eliminated in response to neuro-environmental stimuli (Holtmaat and Svoboda, 2009). However, maintenance of the number of synapses within a certain range, comprising the synapse homeostasis, assures neuronal homeostasis (Davis, 2013; Tien and Kerschensteiner, 2018; Wefelmeyer et al., 2016). It has been proposed that failure of either synapse or neuronal homeostasis results in various neuropsychiatric disorders (Bourgeron, 2009; Ramocki and Zoghbi, 2008). Consistent with this, postmortem pathological studies have revealed that aberrant regulation of dendritic spine number as well as structural abnormalities of spines were observed in patients with numerous psychiatric disorders such as autism spectrum disorders (ASDs), schizophrenia, and neurodegenerative diseases (Hutsler and Zhang, 2010; Penzes et al., 2011; Tang et al., 2014). Thus, appropriate regulation of synaptogenesis as well as synapse homeostasis is critical for normal healthy brain function; however, its molecular machinery remains elusive.

Autism susceptibility candidate 2 (AUTS2) (also termed “activator of transcription and developmental regulator”) located on human chromosome 7q11.22 has been initially identified as a possible ASD risk gene in a study that reported a *de novo* balanced translocation in monozygotic twin patients with ASDs (Sultana et al., 2002). Thereafter, structural variants that disrupt the *AUTS2* locus have been identified in the patients with not only autism but also other neuropathological conditions including intellectual disabilities (IDs), schizophrenia, attention deficit hyperactivity disorder (ADHD), dyslexia, and epilepsy, as well as brain malformation and craniofacial abnormalities (Amarillo et al., 2014; Bakkaloglu et al., 2008; Ben-David et al., 2011; Beunders et al., 2013; Elia et al., 2010; Hori and Hoshino, 2017; Jolley et al., 2013; Kalscheuer et al., 2007; Oksenberg and Ahituv, 2013; Talkowski et al., 2012; Zhang et al., 2014). In addition, *AUTS2* has been recently implicated as a potential gene in human-specific evolution (Oksenberg and Ahituv, 2013; Oksenberg et al., 2013).

¹Department of Biochemistry and Cellular Biology, National Institute of Neuroscience, NCNP, Tokyo 187-8502, Japan

²Department of Neuropsychopharmacology and Hospital Pharmacy, Nagoya University Graduate School of Medicine, Nagoya 466-8560, Japan

³Department of Neuropsychopharmacology, National Institute of Mental Health, NCNP, Tokyo, 187-8502, Japan

⁴Department of Degenerative Neurological Diseases, National Institute of Neuroscience, NCNP, Tokyo, 187-8502, Japan

⁵Cognitive Genomics Research Group, Exploratory Research Center on Life and Living Systems, National Institutes of Natural Sciences, Okazaki, Aichi 444-8585, Japan

⁶School of Life Science, SOKENDAI (The Graduate University for Advanced Studies), Okazaki, Aichi 444-8585, Japan

⁷Department of Physiological Sciences, National Institute for Physiological Sciences, Okazaki, Aichi 444-8585, Japan

⁸Department of Biomolecular Science, Faculty of Science, Toho University, Chiba 274-8510, Japan

⁹Department of Humanities, Faculty of Law, Economics and the Humanities, Kagoshima University, Kagoshima 890-0065, Japan

¹⁰Department of Cellular Neurobiology, Brain Research Institute, Niigata University, Niigata 951-8585, Japan

Continued



We previously reported that the cytoplasmic AUTS2 acts as an upstream regulator for Rho family small GTPases, Rac1 and Cdc42, in reorganizing actin cytoskeleton (Hori et al., 2014). AUTS2 activates Rac1 to induce lamellipodia while downregulating CDC42 to suppress filopodia. In addition to these functions, Gao et al. showed that nuclear AUTS2 binds to and neutralizes the transcriptional repressor activity of Polycomb group (PcG) protein complex 1 (PRC1) and activates some gene transcription by recruiting the histone acetyltransferase P300 into the complex (Gao et al., 2014).

In the developing mouse brain, *Auts2* expression starts from early embryonic stages in multiple regions of the central nervous system, but particularly strong prenatal expression is observed in the regions associated with higher brain functions including neocortex, hippocampus, and cerebellum (Bedogni et al., 2010). We previously demonstrated that the AUTS2-Rac1 signaling pathway is required for neuronal migration and subsequent neurite formation in the developing cerebral cortex (Hori et al., 2014). However, even at postnatal and adult stages, AUTS2 expression is maintained in various types of neurons (Bedogni et al., 2010). Although this late-stage expression raised the possibility that AUTS2 may also be involved in later neurodevelopmental processes, such as synaptogenesis and synaptic homeostasis, its involvement in synapse regulation remains unknown.

In human patients, *AUTS2* mutations are associated with a variety of psychiatric diseases, such as ASD, schizophrenia, depression, intellectual disabilities, and language disability. Although the underlying pathways to evoke this wide range of disorders have not been clarified, one possible mechanism is that different types of gene disruption may cause distinct types of disorders. *AUTS2* is a very large gene with multiple exons and many types of gene mutations, such as deletion, duplication, single nucleotide change, and chromosomal translocation, have been reported in humans (Hori and Hoshino, 2017; Oksenberg and Ahituv, 2013).

In this study, we show that AUTS2 coordinates excitation/inhibition balance by restricting the number of excitatory synapses during development as well as at post-developmental stages. Targeted disruption of *Auts2* resulted in excessive numbers of excitatory synapses without affecting inhibitory ones. Consistent with this, electrophysiological analyses showed that excitatory but not inhibitory inputs increased in the mutant hippocampal neurons where strong c-Fos signals were detected, suggesting impairment in the excitatory and inhibitory coordination in that region. Behavioral analyses on *Auts2* heterozygous mutant mice revealed abnormalities in social interaction and altered vocal communication as well as the defects in recognition. Thus, our data suggest that AUTS2 regulates synapse homeostasis by restricting the number of excitatory synapses without affecting inhibitory ones and that loss of AUTS2 function leads to impaired excitatory and inhibitory coordination that may underlie the pathogenesis of some psychiatric illnesses.

RESULTS

Auts2 Restricts the Number of Excitatory Synapses *In Vitro*

To investigate the involvement of AUTS2 in synapse formation, we utilized primary cultured hippocampal neurons from homozygous *Auts2*-floxed (*Auts2^{fllox/fllox}*) embryos. Most excitatory synapses in mammalian brain are formed on dendritic spines (Bhatt et al., 2009). We confirmed that, at 21 days *in vitro* (DIV21), most PSD-95 (excitatory postsynapse marker) signals were observed on the spine heads (Figure 1A).

Deletion of *Auts2* was carried out by co-introducing GFP with the Cre recombinase expression vector into the *Auts2^{fllox/fllox}* primary hippocampal neurons. Consistent with our previous report, loss of *Auts2* resulted in the impairment of dendrite development, as shown by decreased total dendritic length (**p = 0.003, Figures S1A and S1B). Furthermore, Sholl analysis revealed that the *Auts2*-deficient neurons exhibited a lower dendritic arbor complexity compared with the control neurons (**p = 0.008, Figure S1C) (Hori et al., 2014).

Immunostaining revealed that the *Auts2*-deficient neurons (*Auts2^{del8/del8}* neurons) exhibited a significant increase in the density of dendritic spines compared with the control neurons at DIV28 (***p < 0.001, Figure 1B). Consistent with the increased dendritic spines, *Auts2*-deficient neurons harbored a larger number of excitatory synapses defined as puncta double-positive for PSD-95 and presynaptic marker synapsin-I than the control at DIV21 (**p = 0.001, Figures 1A and 1C). The larger number of excitatory synapses were already evident at an early culture stage (DIV14) in the mutant neurons (***p < 0.001, Figure 1C). Interestingly, the number of inhibitory postsynapse marker, Gephyrin-positive puncta on the dendrites

¹¹Department of Mental Disorder Research, National Institute of Neuroscience, NCNP, Tokyo 187-8502, Japan

¹²Present address: Department of Animal Model development, Brain Research Institute, Niigata University, Niigata 951-8585, Japan

¹³Lead Contact

*Correspondence: khori@ncnp.go.jp (K.H.), hoshino@ncnp.go.jp (M.H.)
<https://doi.org/10.1016/j.isci.2020.101183>

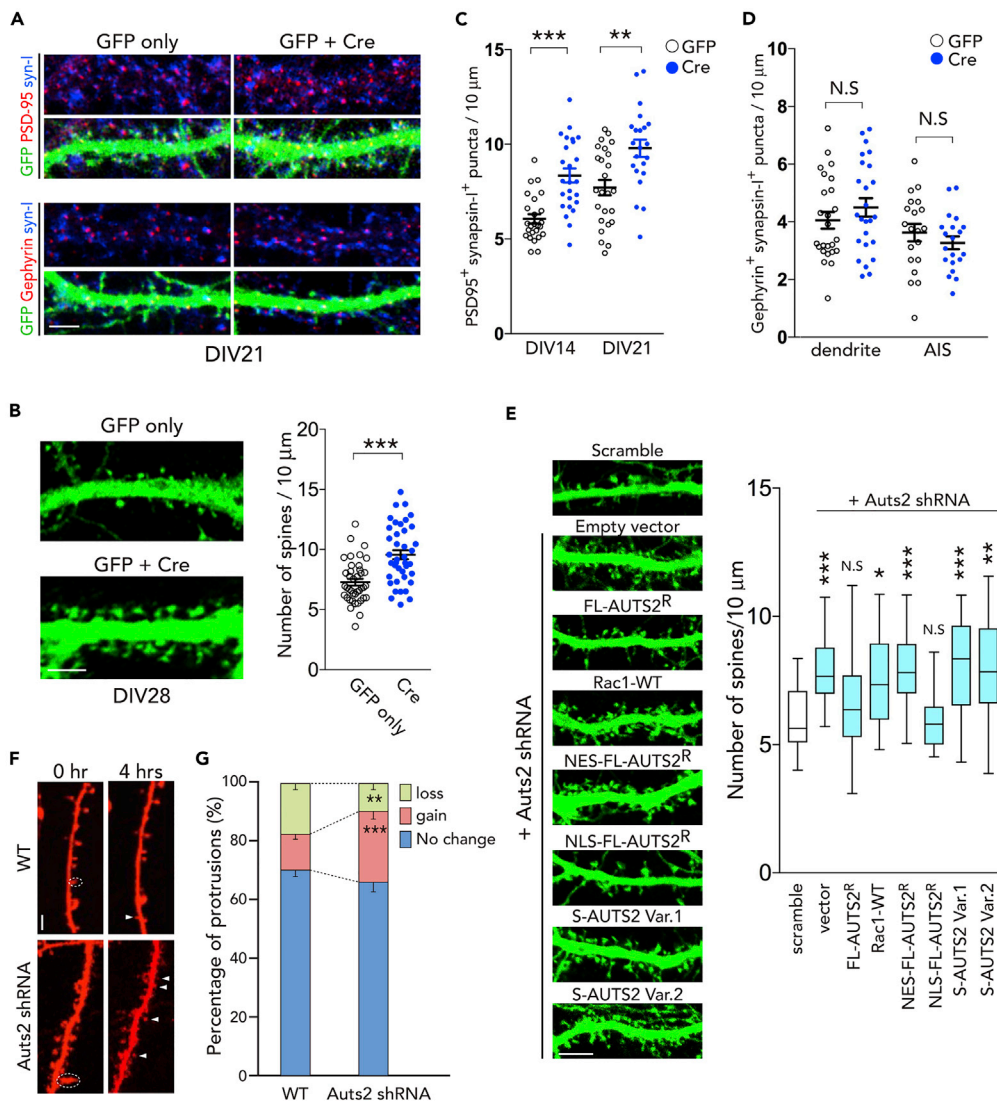


Figure 1. Loss of *Auts2* Induces Excessive Excitatory Synapse Formation

(A) Primary hippocampal neurons derived from *Auts2*^{fllox/fllox} homozygotes at DIV21 were immunolabeled with anti-GFP (green), anti-synapsin I (blue) and anti-PSD-95 or Gephyrin (magenta). Neurons were co-electroporated with control or Cre plus GFP expression vector at DIV0.

(B) Dendritic spines were increased in *Auts2* KO neurons (GFP + Cre) at DIV28. The graph shows the density of dendritic spines in the GFP-positive neurons (n = 40 dendrites from 20 neurons).

(C) The number of PSD-95 puncta colocalized with or adjacent to synapsin-I puncta in GFP-positive cells was measured at DIV14 and 21 (DIV14, n = 28 dendrites; DIV21, n = 51 dendrites of 15–22 neurons).

(D) The number of Gephyrin-positive puncta colocalized with Gephyrin on the dendrites and axon initiation sites (AIS) were measured at DIV21 (n = 25 dendrites and n = 20 AIS of 20 neurons).

(E) WT primary hippocampal neurons were co-electroporated with *Auts2*-shRNA and the indicated expression vectors and analyzed at DIV22–24. To visualize the neurons, GFP vector was co-electroporated. Graph shows the density of dendritic spines (n = 19–20 dendrites). Expression of the shRNA-resistant FL-AUTS2 (FL-AUTS2^R) or nuclear-localized form AUTS2 (NLS-AUTS2^R) in *Auts2*-knockdown neurons rescues the aberrant spine formation.

(F) WT mouse hippocampal neurons at DIV16 expressed with mRFP only (WT) or mRFP plus *Auts2* shRNA vector were imaged at the beginning (0 h) and 4 h after the analysis (dashed white circle, spine eliminated; white arrowheads, spines formed).

(G) Gain and loss of dendritic protrusions (including spines and filopodia) in WT and *Auts2* knockdown neurons were analyzed during a 6-h time window at DIV16–17 (WT, n = 7 neurons; *Auts2* shRNA, n = 10 neurons).

Figure 1. Continued

Data are presented as mean \pm SEM and box-and-whisker plots (medians with interquartile range, minimum, and maximum values are represented). Quantifications in (B)–(E) and (G) represent data from three independent experiments. * $p < 0.05$, ** $p < 0.01$, *** $p < 0.001$, N.S., not significant. (B–D) Unpaired t test; (E) one-way ANOVA with Dunnett's post hoc test; (G) Mann-Whitney U test. Scale bars represent 10 μm .

($p = 0.085$) and axon initial segment (AIS) ($p = 0.343$) as well as the cell somas (WT, $0.086 \pm 0.026/\mu\text{m}^2$ ($n = 20$); KO, $0.090 \pm 0.022/\mu\text{m}^2$ ($n = 20$); data mean \pm SEM, $p = 0.579$, unpaired t test) was not different between the control and *Auts2*-deficient neurons (Figures 1A and 1D). These findings suggest that *Auts2* in postsynaptic cells restricts excessive excitatory synapse formation without affecting inhibitory synapses.

We further observed the development of dendritic spines at different stages in culture (Figure S2A). In control neurons, filopodia were predominantly formed during the first week of culture but gradually decreased from 2 to 4 weeks, with increasing spine formation during the same period. During the first week of culture, *Auts2* mutant neurons had a similar number of protrusions including filopodia and spines as control neurons (Figure S2A: $p = 0.300$ for filopodia, $p = 0.321$ for spine). At later stages, however, larger numbers of dendritic spines as well as filopodia were continuously formed in the *Auts2* mutant neurons compared with the control neurons (Figure S2A: DIV14, *** $p < 0.001$ for filopodia, *** $p < 0.001$ for spine; DIV21, *** $p < 0.001$ for filopodia, *** $p < 0.001$ for spine; DIV28, * $p = 0.039$ for filopodia, *** $p < 0.001$ for spine). The *Auts2*-deficient neurons, however, exhibited the same extent of spine maturation with that of WT neurons, as depicted by the spine maturity index (Figure S2B: DIV7, $p = 0.220$; DIV14, $p = 0.664$; DIV21, $p = 0.903$; DIV28, $p = 0.595$) as well as the spine size (Figure S2C: $p = 0.5903$ for spine length, $p = 0.358$ for spine). Furthermore, we observed no significant difference in the PSD-95 puncta size between the control and *Auts2* mutant neurons ($p = 0.794$, Figure S2D). These results suggest that loss of *Auts2* does not influence the maturation of dendritic spines.

Next, we introduced the expression vectors for AUTS2 isoforms or possible AUTS2 downstream factors into the *Auts2*-knockdown neurons (Hori et al., 2014). We first confirmed that knockdown of *Auts2* well recapitulated aberrant spine formation as observed in *Auts2* KO neurons (Figure 1E: one-way ANOVA, $p < 0.001$, $F_{(6,133)} = 1.781$; Dunnett's post hoc test, *** $p < 0.001$). This abnormality was restored by co-expression of the shRNA-resistant full-length AUTS2 (FL-AUTS2^R), indicating that excess spine formation is the result of specific knockdown of *Auts2* ($p = 0.795$, Figure 1E). We have previously demonstrated that a cytoplasmic AUTS2-Rac1 signaling pathway is required for neuronal migration in the developing cerebral cortex (Hori et al., 2014). In that study, defective cortical neuronal migration in *Auts2* KO mice was shown to be rescued by introduction of either NES (nuclear export sequence)-tagged FL-AUTS2^R (NES-FL-AUTS2^R) (Figure S2E) or wild-type Rac1 (Rac1-WT). Overexpression of these proteins, however, failed to rescue the aberrant spine formation evoked by *Auts2* knockdown (Figure 1E: * $p = 0.013$ for Rac1-WT and ** $p < 0.001$ for NES-FL-AUTS2^R). In contrast, introduction of NLS (nuclear localization signal)-tagged FL-AUTS2^R (NLS-FL-AUTS2^R) (Figure S2E) was able to rescue the spine number to levels comparable with that of control neurons ($p = 0.999$, Figure 1E), whereas the C-terminal AUTS2 short isoforms (S-AUTS2-var.1 and 2) (Figure S3B), which are exclusively localized in nuclei (Hori et al., 2014), were not able to rescue the phenotype (Figure 1E: *** $p = 0.001$ for S-AUTS2-var.1, ** $p = 0.008$ for S-AUTS2-var.2). These results indicate that nuclear FL-AUTS2 is involved in the control of spine number.

In *Auts2*^{delB/delB} brains, expression of FL-AUTS2 and S-AUTS2-var.1 proteins is eliminated, whereas another C-terminal AUTS2 short isoform variant 2 (S-AUTS2-var.2) is increased (Hori et al., 2014), raising a possibility that aberrant synapses in the primary *Auts2*^{delB/delB} hippocampal culture are caused by the overexpression of S-AUTS2-var.2. However, overexpression of S-AUTS2-var.2 into wild-type primary hippocampal neurons did not affect the number and morphology of spines (Figure S2F: one-way ANOVA, $p = 0.521$), suggesting that the formation of aberrant number of spines in *Auts2* mutant neurons was not due to a gain-of-function effect by increased AUTS2 short isoform expression. Similarly, we also found that FL-AUTS2 or S-AUTS2-var.1 did not affect the spine number (Figure S2F).

Next, we performed live imaging to observe the dynamics of dendritic protrusions including spines and filopodia at DIV16–17. During a 6-h time window, neurons expressing the *Auts2* shRNA exhibited a higher rate of protrusion gain (*** $p < 0.001$) and a lower rate of protrusion loss (** $p = 0.002$) compared with WT neurons (Figures 1F and 1G). Compared with the fixed neurons, a higher number of protrusions were formed in the *Auts2*-knockdown living neurons during the time-lapse recording (Figure 1G). This may be attributed to the

difference in experimental conditions. Alternatively, the exposure to laser might have caused damage to living neurons during the time-lapse recording, which may affect the dynamics of cell protrusions.

Altogether, these *in vitro* experiments suggest that AUTS2 restricts the number of excitatory synapses, while not affecting inhibitory neurons.

Loss of *Auts2* Results in Excessive Dendritic Spines *In Vivo*

To assess the involvement of AUTS2 in the regulation of dendritic spine formation *in vivo*, we generated forebrain-specific *Auts2* conditional KO mice by crossing *Auts2*-floxed mice with *Emx1*^{Cre} mice (Iwasato et al., 2000) (Figure S3A and Table S1) and examined brain tissues by Golgi staining to visualize dendrite morphology. Immunoblotting confirmed that expression of FL-AUTS2 protein in the mutant cerebral cortex was successfully eliminated (arrow in Figure S3C).

Spine number generally increases with distance from the cell body in wild-type animals (Ballesteros-Yanez et al., 2006). We examined spine distribution along the middle dendritic segments of pyramidal neurons at multiple forebrain regions in adult brains. We found that spines were increased on the secondary dendrites of layer II/III pyramidal neurons in the medial prefrontal cortex (mPFC) in *Emx1*^{Cre/+};*Auts2*^{flox/flox} homozygous mutant brains compared with the *Auts2*^{flox/flox} controls (one-way ANOVA, $p < 0.001$, $F_{(2,57)} = 14.67$; Dunnett's post hoc test, $***p < 0.001$, Figures 2A and 2B). Significant differences were not limited to mPFC neurons. For example, increased spines were also observed on secondary dendritic segments along apical dendrites of hippocampal CA1 pyramidal neurons and dendrites of the upper-layer neurons of the auditory cortex (Figure 2B: one-way ANOVA, $p < 0.001$, $F_{(2,57)} = 19.02$; Dunnett's post hoc test, $***p < 0.001$ for CA1 apical and Auditory L2/3). Furthermore, we also observed analogous aberrant spine formation along primary apical dendrites immediately proximal to the cell soma of CA1 hippocampal pyramidal neurons as well as cortical layer II/III neurons in the *Auts2* mutant brains, a location where few spines were normally formed in wild-type animals (Figures 2C and 2D: Cortical layer II/III neurons, one-way ANOVA, $p < 0.001$, $F_{(2,39)} = 21.58$; Dunnett's post hoc test, $***p < 0.001$ control versus Het or Homo. CA1 neurons: $p < 0.001$, $F_{(2,36)} = 8.719$; Dunnett's post hoc test, $**p = 0.002$ control versus Het, $**p = 0.001$ control versus Homo). Interestingly, however, spine densities on basal dendrites of CA1 pyramidal neurons as well as both apical and basal dendrites of cortical layer 5/6 neurons at mPFC and auditory cortex were normal in *Auts2* mutant mice (Figure S3D: $p = 0.800$ for CA1 basal, $p = 0.968$ for mPFC L5/6 apical, $p = 0.923$ for mPFC L5/6 basal and $p = 0.923$ for auditory L5/6 basal). These findings suggest that AUTS2 restricts the number of dendritic spines within distinct dendritic compartments in selected neuronal populations. A similar phenotype was observed in *Emx1*^{Cre/+};*Auts2*^{flox/+} heterozygous mutants ($***p < 0.001$, Figure 2B). Furthermore, *Auts2*^{del8/+} heterozygotes at adolescent (P30) as well as adult (P90) stages also displayed an increase in the densities of spines on the dendrites of both cortical and hippocampal CA1 pyramidal neurons compared with WT mouse brains (Figures S4A and S4B: $***p < 0.001$ for mPFC and CA1 neurons at P30, $**p = 0.004$ for mPFC neurons at P90, $***p < 0.001$ for CA1 neurons at P90).

Consistent with the increase of spines, immunohistochemical analysis revealed that the excitatory presynaptic marker VGLUT1 but not inhibitory VGAT-labeled puncta at mPFC was increased in *Auts2* mutant brains compared with the control mice, suggesting that loss of *Auts2* leads to an imbalance of excitatory and inhibitory synapse density (Figure S5: $***p < 0.001$ for VGLUT1, $p = 0.070$ for VGAT).

We categorized spines into four morphological types (Figure 2E) and found that both mature "mushroom" spines and immature "thin" spines were increased to a similar extent in dendrites of *Emx1*^{Cre/+};*Auts2*^{flox/+} heterozygous and *Emx1*^{Cre/+};*Auts2*^{flox/flox} homozygous or *Auts2*^{del8/+} mice (Figures 2F and S4C: Thin spine, one-way ANOVA, $p < 0.001$, $F_{(2,57)} = 12.87$; Dunnett's post hoc test, $***p < 0.001$ control versus Het or Homo. Mushroom spine, one-way ANOVA, $p < 0.001$, $F_{(2,57)} = 10.67$; Dunnett's post hoc test, $***p = 0.002$ control versus Het, $***p < 0.001$ control versus Homo). This indicates that AUTS2 does not affect the maturity of spines, as was also observed in our *ex vivo* data (Figures S2B–S2D). These observations suggest that AUTS2 restricts the number of excitatory synapses and that loss of one allele is sufficient to result in excessive excitatory synapses.

Auts2 Deficiency Causes Aberrant Excitatory Neurotransmission

Next, we investigated the effect of *Auts2* inactivation on synaptic transmission properties. To address this, we performed whole-cell patch clamp recording of spontaneous miniature excitatory and inhibitory

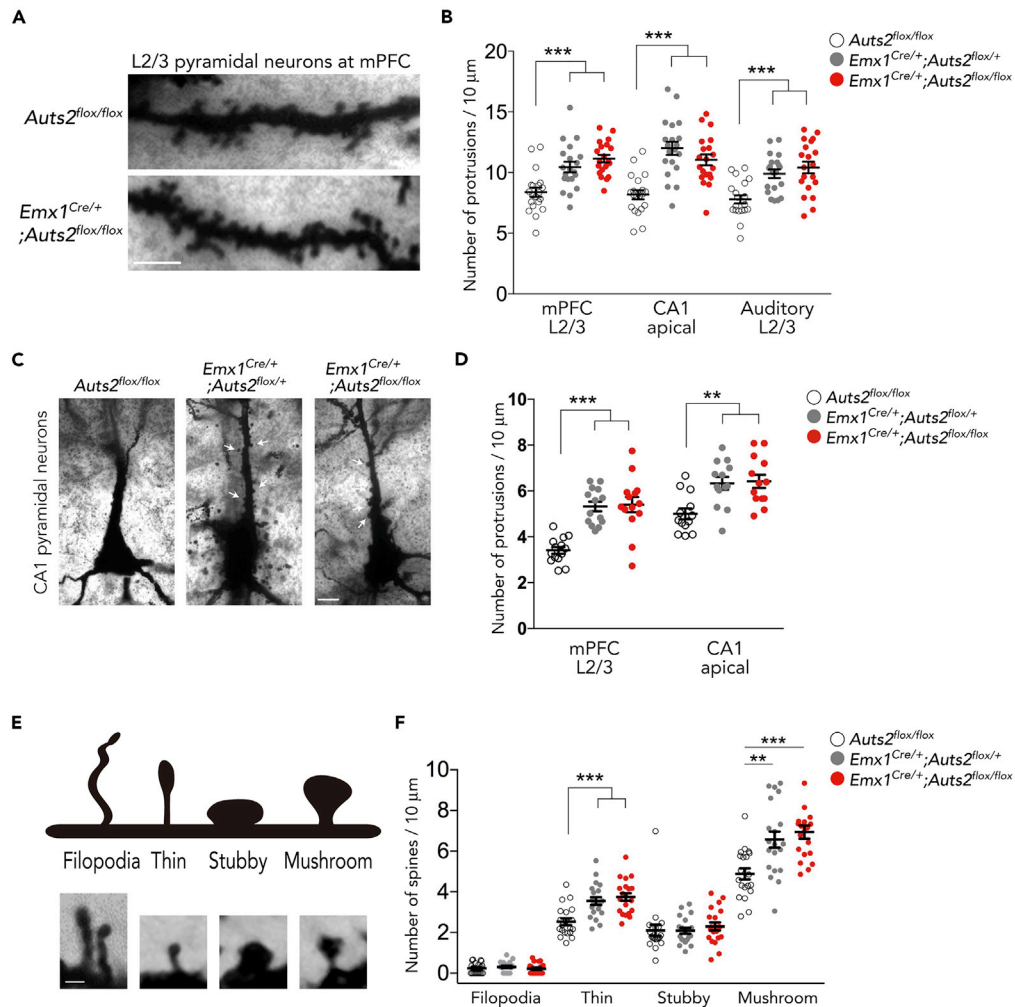


Figure 2. Loss of *Auts2* Abnormally Increases Dendritic Spine Formation *In Vivo*

(A) Representative images of spines on the secondary dendritic segments from Golgi-stained upper-layer pyramidal neurons in the mPFC of control (*Auts2^{flox/flox}*, upper panel) and *Emx1^{Cre/+};Auts2^{flox/flox}* homozygous mutant mouse brains (lower panel) at P35.

(B) Summary graph of the spine density on the neurons at indicated areas in the control (*Auts2^{flox/flox}*), heterozygous (*Emx1^{Cre/+};Auts2^{flox/+}*), and homozygous (*Emx1^{Cre/+};Auts2^{flox/flox}*) mutant mouse brains (n = 20 dendrites from n = 3 animals).

(C) The representative images of Golgi-stained CA1 hippocampal pyramidal neurons in *Auts2^{flox/flox}*, *Emx1^{Cre/+};Auts2^{flox/+}* heterozygotes, and *Emx1^{Cre/+};Auts2^{flox/flox}* homozygotes at P35. *Auts2* mutant neurons exhibited increased spines at apical primary dendrites (white arrows).

(D) Summary graph of the spine density at apical primary dendrites on neurons in control (*Auts2^{flox/flox}*), heterozygous (*Emx1^{Cre/+};Auts2^{flox/+}*), and homozygous (*Emx1^{Cre/+};Auts2^{flox/flox}*) mutant mouse brains (n = 13–15 dendrites from n = 3 animals).

(E) Morphological classification of dendritic spines and filopodia.

(F) The density of each category of spines in the upper-layer neurons in the mPFC was measured in the control (*Auts2^{flox/flox}*), heterozygous (*Emx1^{Cre/+};Auts2^{flox/+}*), and homozygous (*Emx1^{Cre/+};Auts2^{flox/flox}*) mutant mouse brains (n = 20 dendrites from n = 3 animals).

Data are presented as mean \pm SEM. **p < 0.01, ***p < 0.001, one-way ANOVA with Dunnett's post hoc test. Scale bar, 10 μ m (A and C) and 2 μ m (B).

postsynaptic currents (mEPSCs and mIPSCs, respectively) on CA1 pyramidal neurons in acute hippocampal slices from P33–44 mouse brains. In the *Emx1^{Cre/+};Auts2^{flox/flox}* homozygous brains, the mEPSCs were increased in frequency (**p = 0.006), in agreement with increased spines (Figures 3A and 3C). Furthermore, the average paired-pulse ratio of evoked EPSCs in response to paired sets of local stimulation was

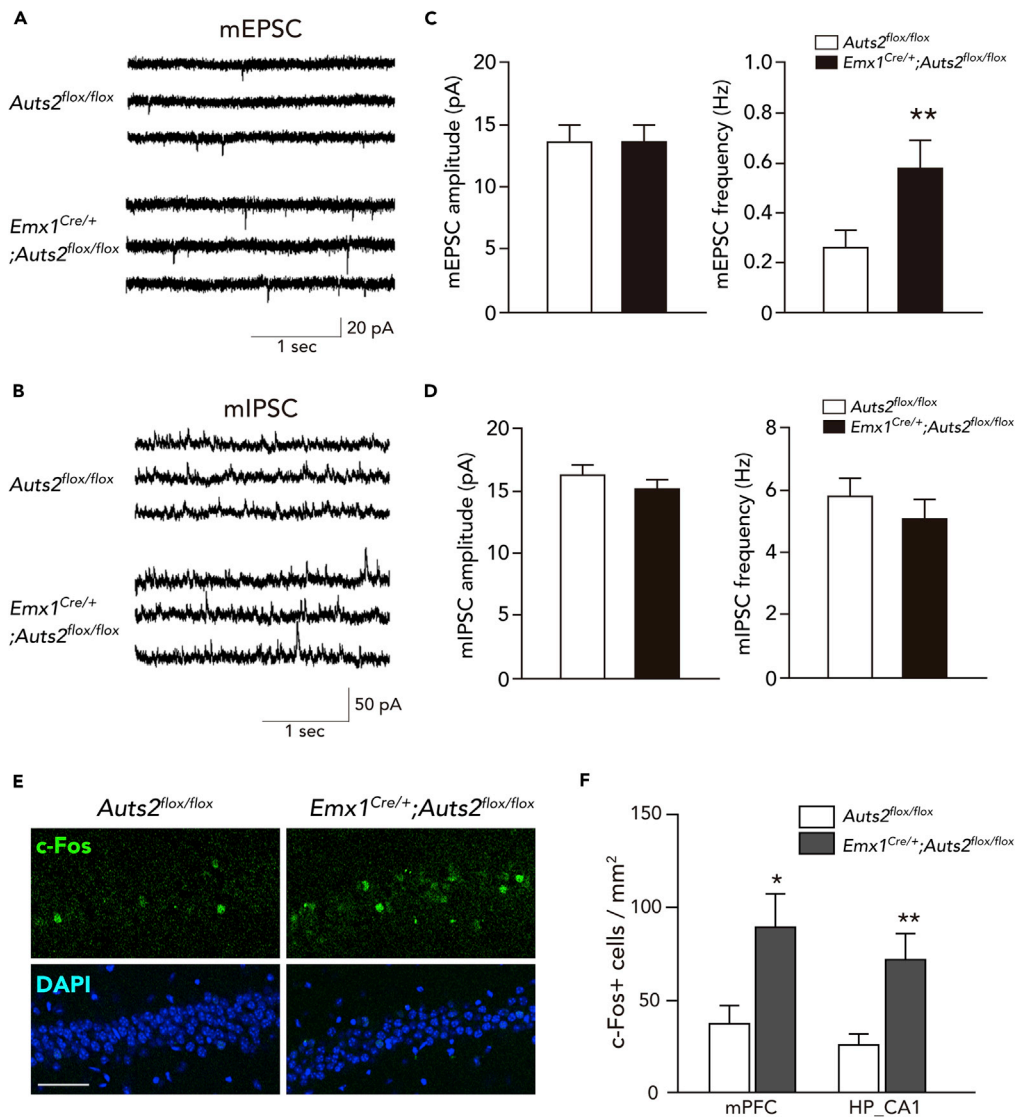


Figure 3. *Auts2* Mutant Mice Display Altered Synaptic Properties and Increased c-Fos Expression

(A and B) Representative traces of mEPSCs (A) and mIPSCs (B) from slice recordings of CA1 pyramidal neurons from control (*Auts2^{flox/flox}*) and *Emx1^{Cre/+};Auts2^{flox/flox}* homozygous mutant mice at P35.

(C and D) *Emx1^{Cre/+};Auts2^{flox/flox}* mice exhibit increased mEPSC (C) but not mIPSC (D) frequencies without change in amplitude. n = 18–19 neurons from N = 6–8 mice per genotype.

(E) Representative images of c-Fos expression in the hippocampal CA1 areas of homozygous *Emx1^{Cre/+};Auts2^{flox/flox}* homozygous mutant mice and *Auts2^{flox/flox}* control littermates.

(F) Summary graphs of c-Fos-expressing cells in the indicated areas. About 8–12 tissue sections from N = 3 brains were analyzed.

Data are presented as mean ± SEM. *p < 0.05, **p < 0.01, Mann-Whitney U test. Scale bar, 50 μm.

unchanged across the genotypes (p = 0.520, Figure S6), suggesting that the increase in mEPSC frequency observed in *Auts2* mutant brains is probably due to an increase in the number of functional excitatory synapses rather than an increase in the probability of presynapse release. On the other hand, the mEPSC in amplitude was unaltered (p = 0.954) compared with the control (*Auts2^{flox/flox}*) mice (Figures 3A and 3C), suggesting that ablation of *Auts2* does not further promote the maturation of excitatory synapses. We also observed no significant difference in the mIPSCs with regard to either amplitude or frequency between the control and *Emx1^{Cre/+};Auts2^{flox/flox}* mutants (Figures 3B and 3D: p = 0.171 for amplitude, p = 0.252 for frequency).

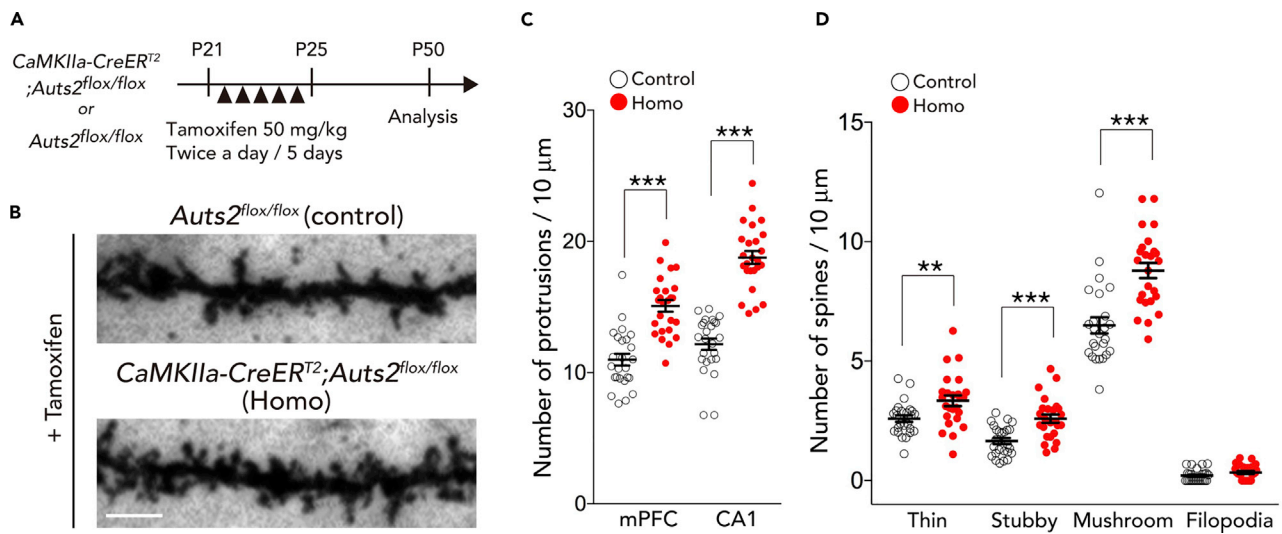


Figure 4. Conditional Deletion of *Auts2* in Postnatal Forebrain Leads to Excessive Spine Formation

(A) Scheme illustrating the tamoxifen-inducible deletion of *Auts2* in postnatal forebrain. Tamoxifen was administered to *CaMKIIa-CreER^{T2};Auts2^{flox/flox}* homozygotes and their control *Auts2^{flox/flox}* littermate mice during P21–25, and analysis was performed at P50. (B) Representative images of the dendritic spines from Golgi-stained upper-layer pyramidal neurons at mPFC of the tamoxifen-treated control (*Auts2^{flox/flox}*, upper panel) and *Auts2* homozygous mutant mouse brains (*CaMKIIa-CreER^{T2};Auts2^{flox/flox}*, lower panel) at P50. (C) The pyramidal neurons in the mPFC as well as hippocampal CA1 area from mice postnatally lacking *CaMKIIa-CreER^{T2};Auts2^{flox/flox}* (Homo) exhibited increase of dendritic spines on the secondary dendritic segments relative to the *Auts2^{flox/flox}* littermates (control) ($n = 25$ dendrites from $N = 3$ animals). (D) The density of each category of spines on the pyramidal neurons in the mPFC was measured in control (*Auts2^{flox/flox}*) and homozygous *CaMKIIa-CreER^{T2};Auts2^{flox/flox}* mutant mouse brains ($n = 25$ dendrites from $N = 3$ animals). Data are presented as mean \pm SEM. ** $p < 0.01$, *** $p < 0.001$, unpaired t test. Scale bar, 10 μ m.

Furthermore, we examined the expression of the immediate-early gene product, c-Fos, as a marker of neuronal activity in the brain (Sagar et al., 1988). Compared with the control (*Auts2^{flox/flox}*) mice, a larger number of pyramidal neurons with strong c-Fos immunoreactivity were observed in the mPFC and hippocampal CA1 in *Emx1^{Cre/+};Auts2^{flox/flox}* homozygous mutants (Figures 3E and 3F: * $p = 0.023$ for mPFC, ** $p = 0.009$ for CA1). This suggests that the disturbed balance between excitatory and inhibitory synaptic inputs in local neural circuits results in increased excitability in the *Auts2* mutant brains.

***Auts2* Prevents Excessive Spine Formation Even after Developmental Stages**

Although our *ex vivo* and *in vivo* analyses suggest that AUTS2 regulates excitatory synapse formation, it is unclear whether AUTS2 possesses such a function after establishment of brain structures. To assess this issue, we crossed *Auts2*-floxed mice with *CaMKIIa-CreER^{T2}* mice to generate *CaMKIIa-CreER^{T2};Auts2^{flox}* mutant mice, in which the exon 8 of *Auts2* can be ablated in the forebrain projection neurons by administration of tamoxifen (Erdmann et al., 2007) (Figure S7A and Table S1). We have previously demonstrated that *Auts2* mutant mice displayed defects in neural development including neuronal migration and neurite outgrowth in a gene-dosage dependent manner (Hori et al., 2014, *Cell Rep*). Interestingly, however, the *Emx1^{Cre/+};Auts2^{flox/+}* heterozygous mutants exhibited aberrant spine formation to the same extent as the homozygotes (Figure 2B: $p = 0.394$ Het (*Emx1^{Cre/+};Auts2^{flox/+}*) versus Homo (*Emx1^{Cre/+};Auts2^{flox/flox}*) for mPFC; $p = 0.305$ Het versus Homo for CA1; $p = 0.631$ Het versus Homo for CA1, one-way ANOVA with Bonferroni post hoc test). To better understand the contribution of AUTS2 in postnatal synapse development as well as the *Auts2* phenotypes on mouse behaviors as described below, we examined *CaMKIIa-CreER^{T2};Auts2^{flox/flox}* homozygotes and *Auts2^{flox/flox}* control mice (Figures 4 and S11).

Tang et al. previously demonstrated that the *CaMKIIa*-promoter is active in forebrain neurons from postnatal week 3 to adulthood (Tang et al., 2014). When tamoxifen was administered during P21–25 to *CaMKIIa-CreER^{T2};Auts2^{flox/flox}* mutant mice and their control littermates (*Auts2^{flox/flox}*), genomic recombination was detected in the mPFC and hippocampus but not in the cerebellum of *CaMKIIa-CreER^{T2};Auts2^{flox/flox}* mice (Figure S7B), indicating that this protocol efficiently induces the forebrain-specific Cre-mediated recombination. Induction of recombination was also confirmed by using *Rosa26^{YFP}*, a reporter allele to

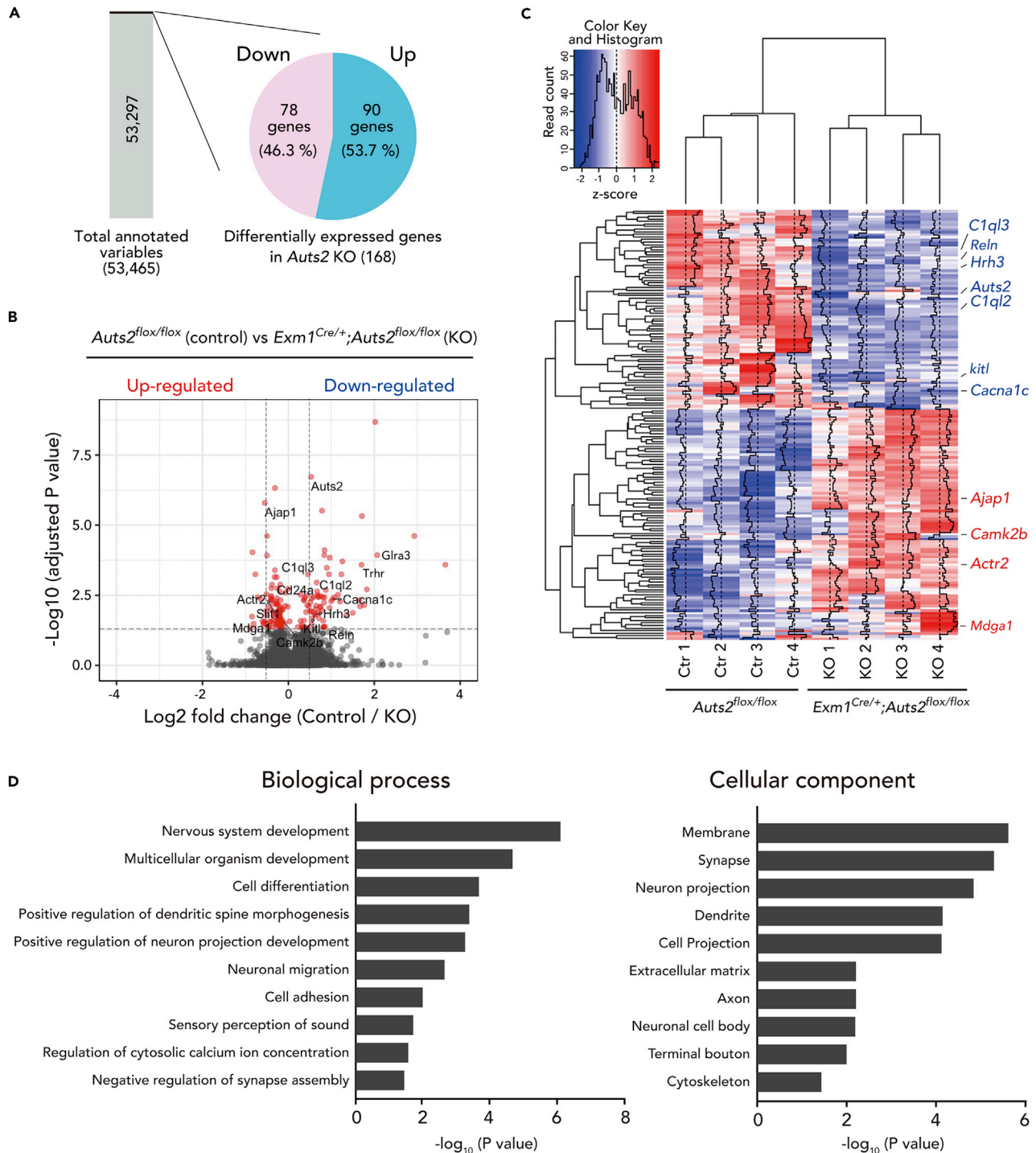


Figure 5. Continued

(C) Clustered heatmap of transcriptome analysis in *Emx1^{Cre/+};Auts2^{fllox/fllox}* homozygous mutants (KO) and the *Auts2^{fllox/fllox}* control littermates (Ctr). Four biological samples as indicated were subjected to RNA-seq analysis. Heatmap was generated by Z score calculated with the processed FPKM values for each differentially expressed gene.

(D) Gene ontology (GO) analysis of the differentially expressed genes in *Auts2* mutant hippocampus.

detect Cre-dependent recombination (Figure S7C). Quantitative RT-PCR revealed that *Auts2* mRNA levels dramatically decreased in the mPFC and hippocampus but not in the cerebellum of the tamoxifen-treated *CaMKIIa-CreER^{T2};Auts2^{fllox/fllox}* mice (Figure S7D: ***p < 0.001 for mPFC, **p = 0.001 for HP, p = 0.054 for Cb).

Three weeks after tamoxifen administration to *CaMKIIa-CreER^{T2};Auts2^{fllox/fllox}* homozygous mutants and *Auts2^{fllox/fllox}* control mice (Figure 4A), *CaMKIIa-CreER^{T2};Auts2^{fllox/fllox}* mice displayed an increase in the densities of spines on the dendrites of both cortical and hippocampal pyramidal neurons (Figures 4B and 4C: ***p < 0.001 for mPFC neurons, ***p < 0.001 for CA1 neurons). Similar to the *Emx1^{Cre/+};Auts2^{fllox/fllox}* mutant mice, those increased spines consisted of mushroom and stubby-type mature spines as well as immature thin spines (Figure 4D: **p = 0.007 for thin spine, ***p < 0.001 for stubby spine, ***p < 0.001 for mushroom spine, p = 0.098 for filopodia). These findings suggest that AUTS2 is required for the dendritic spine number restriction even at post-developmental stages, which may contribute to the regulation of synaptic homeostasis.

Aberrant Gene Expression in *Auts2* Mutant Mice

The *ex vivo* rescue experiments in Figure 1E showed that AUTS2 in the nucleus functions to restrict the spine number. A previous study clarified that nucleic AUTS2 works as a component of PRC1 to participate in gene transcription (Gao et al., 2014). These findings suggest that AUTS2 protein in nuclei restricts spine formation by regulating gene expression of relevant neural genes. Therefore, we examined global mRNA expression profiles for *Emx1^{Cre/+};Auts2^{fllox/fllox}* homozygous brains and *Auts2^{fllox/fllox}* control littermate brains. In the postnatal mouse brains, the expression of AUTS2 in the cerebral cortex is downregulated to considerably lower levels and is confined to the prefrontal regions (Bedogni et al., 2010). In addition, the disturbed spine formation elicited by the ablation of *Atus2* is specific to the upper-layer neurons in the cerebral cortex (Figures 2B and S3D). In contrast, the hippocampus entirely sustains a higher level of AUTS2 expression even in mature brains. Thus, we prepared the RNA samples from the hippocampi of 2-week-old *Auts2* homozygous mutants and the control littermates for RNA sequencing (RNA-seq) analysis. Through RNA-seq, we identified a total of 168 genes, whose expression levels were significantly altered (false discovery rate [FDR] < 0.05) in the mutant hippocampus, with 78 downregulated and 90 up-regulated genes expressed as Log₂FKPM (fragments per kilobase of exon per million reads mapped) (Figures 5A–5C and Data S1). Interestingly, these differentially expressed genes included the genes encoded synaptic proteins or molecules involved in synaptic functions, such as *Reln*, *Mdga1*, *Camk2b*, *Cacna1c*, and *C1ql*-family genes (Fink et al., 2003; Gangwar et al., 2017; Martinelli et al., 2016; Matsuda et al., 2016; Moosmang et al., 2005; Pettem et al., 2013; van Woerden et al., 2009; Wasser and Herz, 2017) (Figures 5B and 5C). Gene ontology (GO) analysis revealed that these altered genes were associated with multiple aspects of neurodevelopment including “nervous system development,” “cell differentiation,” and “neuronal migration,” with particular enrichment of the terms for synapse development such as “dendritic spine morphogenesis,” “negative regulation of synapse assembly,” and “regulation of cytosolic calcium ion concentration” (Figure 5D and Data S2). Among the genes categorized in GO cellular components such as “Membrane” or “Synapse,” six up-regulated (e.g., *Mdga1*, *Camk2b*, and *sema6b*) and thirteen down-regulated genes (e.g., *Dcc*, *Gfra1*, *Gpc2*, *Hap1*) overlapped with genes categorized in the biological process “nervous system development” (Figure S8). These results suggest that nucleic AUTS2 regulates the expression of genes that are related to synapse formation/function and some of which may be involved in spine number restriction. Aberrant expression of such synaptic genes may cause synaptic dysfunction in patients with *AUTS2* mutations.

Loss of *Auts2* Impairs Social Behaviors

In our previous studies, the heterozygotic mouse mutants for another *Auts2* allele, *Auts2^{neo/+}*, whose AUTS2 expression profile is distinct from that of *Auts2^{delB/+}* (Table S1), displayed the behavioral abnormalities in cognition and emotional control while behaving normally in social interaction (Hori et al., 2014, 2015). Human genetic studies have previously reported that individuals with mutations in *AUTS2* locus

exhibited common features including ID, developmental delay, microcephaly, and epilepsy but distinct psychiatric disorders such as ASDs, ADHD, and schizophrenia (Oksenberg and Ahituv, 2013). One plausible hypothesis is that the heterogeneity of structural variants in the *AUTS2* locus could result in the expression of phenotypic variation between the patients with *AUTS2* mutations. This prompted us to examine the social behaviors of *Auts2*^{delB/+} mice, especially focusing on mouse social communications.

All experimental mice including *Auts2*^{delB/+} mutants, tamoxifen-treated *CaMKIIa-CreER*^{T2};*Auts2*^{flox/flox} mice, and *Auts2*^{flox/flox} control littermates appeared grossly normal. All of them had normal fur and whiskers and showed no detectable motor disability. The body weight of *Auts2*^{delB/+} mice was slightly decreased compared with WT littermates (body weight at 3 months of age; WT, 27.94 ± 0.54 g [n = 16]; *Auts2*^{delB/+}, 20.50 ± 0.35 [n = 16]; data are mean ± SEM, Mann-Whitney *U* = 2.5, ****p* < 0.001).

We performed the reciprocal dyadic social interaction test to evaluate social behavior, in which mice were allowed to freely move and reciprocally interact with each other (Harper et al., 2012; Hiramoto et al., 2011). *Auts2*^{delB/+} mice displayed lower levels of active affiliative social interaction than WT mice in both session 1 and session 2 (Figure 6A: ***p* = 0.001 for session 1, ***p* = 0.009 for session 2). Of note, the restricted ablation of *Auts2* in mature excitatory neurons in the adult forebrain well recapitulated the impairment of social interaction, as depicted by tamoxifen-treated *CaMKIIa-CreER*^{T2};*Auts2*^{flox/flox} mutants (Figures S11A and S11D: ***p* = 0.001 for session 1, **p* = 0.038 for session 2). Furthermore, in a three-chamber social interaction test, *Auts2*^{delB/+} mutant mice displayed a decreased preference for a social subject (stranger mice 1 and 2) over non-social subject (empty chamber or familiar mouse) compared with WT mice in both sociability and social novelty phases (Figure 6B). These results suggest that *Auts2* mutant mice have social defects. We confirmed that sensory abilities such as olfaction and visual functioning as well as tactile response were not significantly different across the genotypes, as no phenotype was observed in the buried food finding test (Figure S9A: *p* = 0.065; Figure S11C: *p* = 0.707), whisker twitch reflex (100% response in WT, n = 12, *Auts2*^{delB/+}, n = 10, *Auts2*^{flox/flox}, n = 10 and *CaMKIIa-CreER*^{T2};*Auts2*^{flox/flox}, n = 10), and visual placing response test (*p* = 0.898, Figure S9B; *p* = 0.557, Figure S11B), respectively. To further examine the sensory function of the vibrissae, we measured thigmotactic behaviors, defined as movement along the walls so that one side of the vibrissae could contact and scan the edge of the wall (Luhmann et al., 2005; Milani et al., 1989). *Auts2*^{delB/+} mutant and WT mice behaved similarly in this test (Figure S9C: time × genotype interaction, *F*_(3,54) = 0.337, *p* = 0.799; genotype, *F*_(1,18) = 0.670, *p* = 0.424; time, *F*_(3,54) = 4.06, *p* = 0.011). These results suggest that the impaired social interaction probably does not involve the alterations in non-specific elements of social behavior such as sensory functioning.

Other Behavioral Phenotypes of *Auts2*^{delB/+} Mice

Spontaneous locomotor activity test showed that the *Auts2*^{delB/+} mice exhibited significantly decreased exploratory behavior during the first 15 min of the test (Figure S10A: time × genotype interaction, *F*_(2,66) = 7.61, *p* = 0.001; genotype, *F*_(1,33) = 21.68, *p* < 0.001; time, *F*_(2,66) = 5.07, *p* = 0.009).

In the open field test, the time that *Auts2*^{delB/+} mice spent in the illuminated inner area was comparable with that of WT mice, although general locomotor activity was slightly reduced in *Auts2*^{delB/+} mice as indicated by total travel distance during the test (Figure S10B: time spent in inner sector, *p* = 0.697; total distance traveled, ****p* < 0.001). In the elevated plus maze test, however, *Auts2*^{delB/+} mice displayed increased exploratory behavior of the open arms compared with WT mice, suggesting that *Auts2*^{delB/+} mice have reduced fear of height (***p* = 0.008, Figure 6C).

In a novel object recognition test, *Auts2*^{delB/+} mice exhibited impaired recognition memory performance depicted by the significant decrease of time for exploratory index to the novel object (Figure 6D: session × genotype interaction, *F*_(1,62) = 25.63, *p* < 0.001; genotype, *F*_(1,62) = 25.15, *p* = 0.001; session, *F*_(1,62) = 21.74, *p* < 0.001). Meanwhile, *Auts2*^{delB/+} mice showed normal associative memory functions in the fear-conditioning test (Figure S10C: context-dependent, *p* = 0.175; tone-dependent, *p* = 0.841). Interestingly, *Auts2*^{delB/+} exhibited a higher response to nociceptive stimuli as observed in the *Auts2*^{neo/+} mutants in our previous study (***p* < 0.001, Figure S10C) (Hori et al., 2015). Furthermore, *Auts2*^{delB/+} exhibited abnormal acoustic startle responses as well as sensorimotor gating deficits as indicated by decrease in the percentage of prepulse inhibition (Figure 6E: prepulse × genotype interaction, *F*_(3,93) = 3.31, *p* < 0.023; genotype, *F*_(1,31) = 19.77, *p* < 0.001; prepulse, *F*_(3,93) = 74.83, *p* < 0.001 for PPI; *p* = 0.103 for startle response to a 60 dB, ****p* < 0.001 for startle response to a 120 dB).

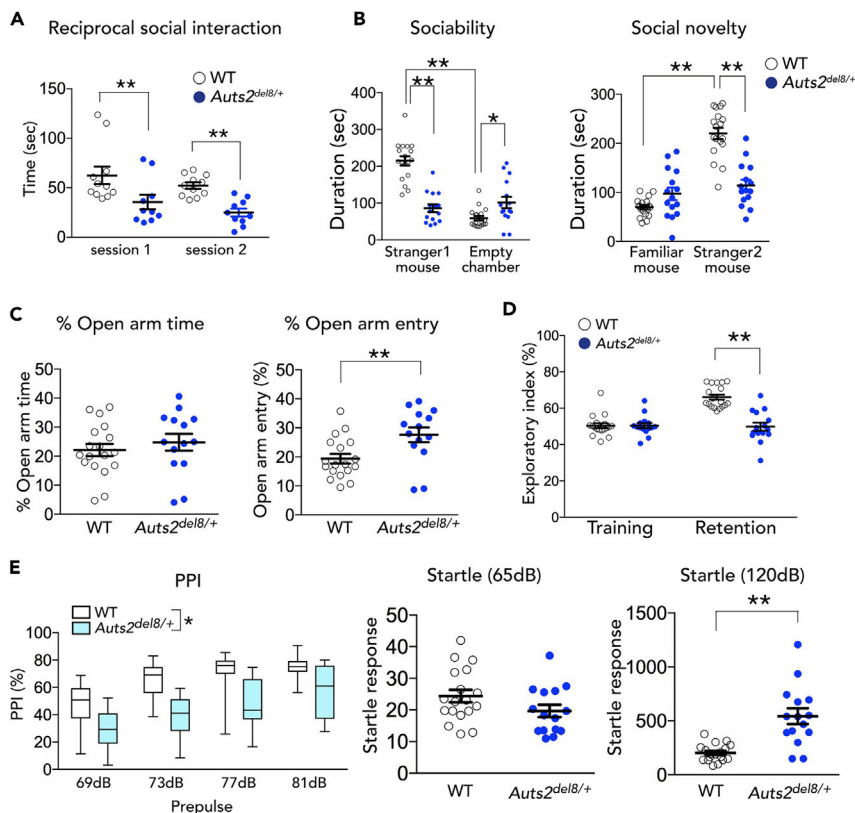


Figure 6. Behavioral Abnormalities in *Auts2^{del18/+}* Mutant Mice

(A) Reciprocal social interaction test. Social interaction between WT or *Auts2^{del18/+}* mouse pairs during 5 min were measured (WT, n = 11, *Auts2^{del18/+}*, n = 10).
 (B) Three-chamber social interaction test. Graphs show the amount of time spent in each chamber (WT, n = 18, *Auts2^{del18/+}*, n = 15).
 (C) *Auts2^{del18/+}* mice exhibit increased open arm entry relative to WT mice in elevated plus maze test (WT, n = 18, *Auts2^{del18/+}*, n = 14).
 (D) *Auts2^{del18/+}* mice display deficits in novel object recognition. Graphs show the exploratory preference in training and retention sessions (WT, n = 18, *Auts2^{del18/+}*, n = 15).
 (E) Prepulse inhibition (PPI) (%) at four different prepulse intensities in PPI test (left graph) and acoustic startle response (middle and right graphs) as measured in trials without a prepulse. *Auts2^{del18/+}* mice display decrease of the percentage of PPI as well as a higher acoustic startle response at 120 dB pulse relative to those in WT mice (WT, n = 18, *Auts2^{del18/+}*, n = 15).

Data are mean \pm SEM and box-and-whisker plots (medians with interquartile range, minimum, and maximum values are represented). *p < 0.05, **p < 0.01; (A and B) two-way ANOVA, (C) unpaired t test, (D) two-way ANOVA with repeated measures, (E) two-way ANOVA with repeated measures in PPI test and Mann-Whitney U-test in startle response.

Altered Vocal Communication in *Auts2* Mutant Mice

Among types of social behaviors, mouse vocal communication has recently received attention as a possible model for studying the genetic and neural mechanisms for social communication (Holy and Guo, 2005). Mice use ultrasonic vocalizations (USVs) to exchange information in a variety of social contexts (Portfors and Perkel, 2014). When interacting with females, adult WT males actively emit courtship USVs with key tone frequencies between 50 and 80 kHz, as observed in the real-time spectrograms in Figure 7A. In contrast, the USVs produced by *Auts2^{del18/+}* males were apparently dispersive during the test (Figure 7A). Indeed, the mean number and duration of USVs were markedly reduced in *Auts2^{del18/+}* mice compared with WT controls (Figure 7B: ***p < 0.001 for call number; ***p < 0.001 for duration). Similarly, *CaMKIIa-CreER^{T2};Auts2^{flox/flox}* males also displayed the altered vocalizations (Figure S11E: **p = 0.003 for call number; p = 0.058 for duration). The experiments of auditory playback previously showed that adult females prefer USVs with greater complexity from neonates as well as adult males (Chabout et al., 2015; Takahashi et al., 2016). We classified the acoustic structures of USVs into 12 different call patterns and grouped them into “simple”

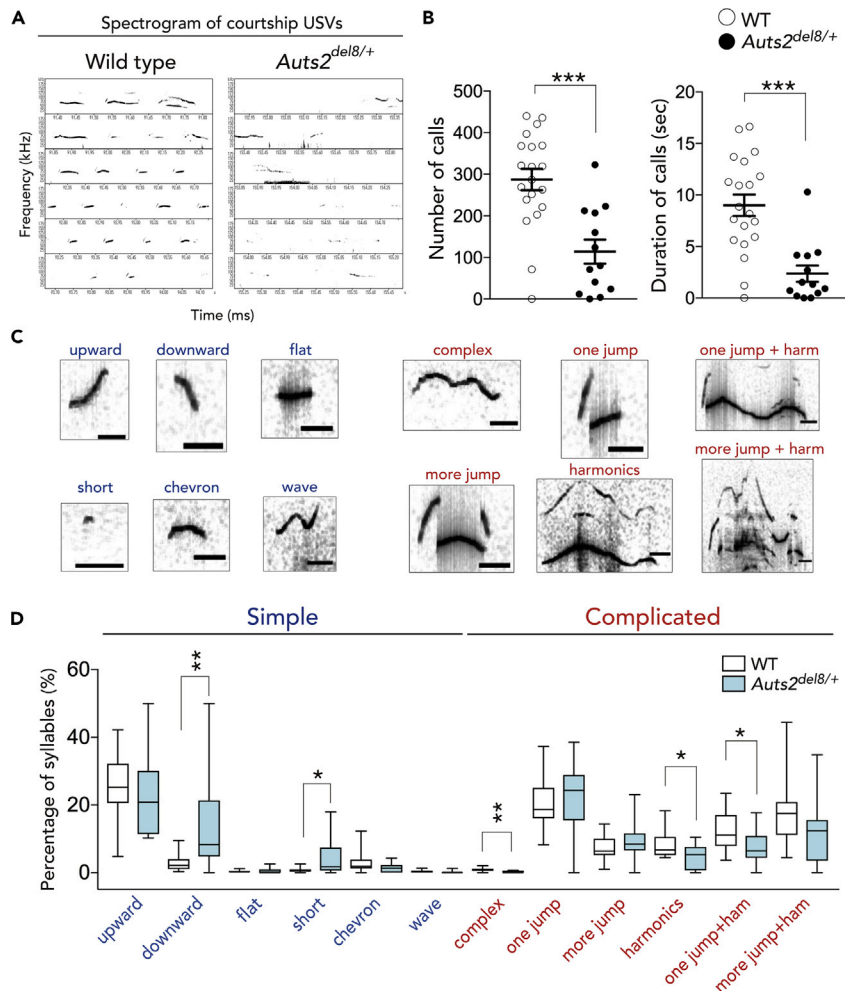


Figure 7. Deficits in Vocal Communication in Adult *Aut2^{delB/+}* Mutant Mice

(A) Representative spectrograms of USV during the courtship behaviors.

(B) The number (left) and duration (right) of USVs during 1 min.

(C) Typical spectrograms of 12 different call patterns. Six simple call types (blue) and six complicated call types (red) are indicated.

(D) The frequency of each syllable pattern is shown as the percentage of total calls.

Data are mean \pm SEM and box-and-whisker plots (medians with interquartile range, minimum, and maximum values are represented) (WT, n = 20, *Aut2^{delB/+}*, n = 13). *p < 0.05, **p < 0.01, ***p < 0.001; (B) unpaired t test, (D) Mann-Whitney U test.

and “complicated” syllable types (Figure 7C). *Aut2^{delB/+}* emitted significantly fewer numbers of the complicated syllable type, including “harmonics,” “complex,” or “one jump + harmonics,” whereas the simple syllable types with shorter duration such as “downward” or “short” were significantly increased (Figure 7D: **p = 0.002 for downward; *p = 0.025 for short; **p = 0.001 for complex; *p = 0.022 for harmonics; *p = 0.025 for one jump + harmonics). These findings suggest that loss of *Aut2* alters mouse vocal communication, which may underlie the pathology for communication disorders in patients with ASD with *AUTS2* mutations.

DISCUSSION

In this study, we found that *AUTS2* restricts the number of excitatory synapses in forebrain pyramidal neurons, such as mPFC, and in the hippocampus, which are implicated as the critical regions for socio-communicative and cognitive brain functions. In *Aut2* mutant forebrains, the aberrant dendritic spine formation leads to the enhancement of excitatory synaptic inputs, which results in the changes in a balance between

excitation and inhibition (E/I) that is observed in several otherwise different neuropsychiatric disorders such as ASDs and schizophrenia as well as mouse models (Lee et al., 2017; Penzes et al., 2011). These findings suggest a potential link between the behavioral abnormalities in *Auts2* mutant mice and the aberrant dendritic spine development.

Interestingly, in *Auts2* mutant cerebral cortex, aberrant spine formation specifically appeared in the upper-layer but not deep-layer neurons, although AUTS2 is widely expressed in both cortical layers (Figures 2B and S3D) (Bedogni et al., 2010). One plausible hypothesis is that AUTS2 may have distinct roles for neural development in different cerebral cortical areas, which may depend on differences of AUTS2 isoforms expressed between neurons or on co-factors that differentially interact with each AUTS2 isoform. Monderer-Rothkoff et al. have recently demonstrated that the long and short AUTS2 isoforms, each interacting with different co-factors, act opposingly on gene transcription in a cellular-context-dependent manner (Monderer-Rothkoff et al., 2019).

Electrophysiological experiments revealed that excitatory but not inhibitory synaptic inputs were elevated in the *Auts2* mutant hippocampal slices where strong c-Fos signals were observed, implying that the E/I balance was disturbed in that region. E/I balance in neural circuits is tightly controlled and established by contributions from a large number of factors in the normal brain. Accumulating evidence implicates a disturbed E/I balance within cortical neural circuitry in various neuropsychiatric disorders including ASD, anxiety, and ADHD (Chao et al., 2010; Edden et al., 2012; Gogolla et al., 2009; Han et al., 2012; Rubenstein and Merzenich, 2003). Although a recent report suggests that E/I imbalance is not causative for the neuropathology of the disorders but reflects a homeostatic response in some mouse models (Antoine et al., 2019), the hyperexcitability caused by an increased E/I ratio in the cerebral cortex is thought to be one potential common mechanism underlying the neurobehavioral defects of some forms of ASD via a distinct molecular pathway (Lee et al., 2017).

During the spinogenesis, a rapid increase of dendritic spine density occurs in the forebrain neurons, in which the gain of spines exceeds loss of spines, eventually causing excessive excitatory synapses for the formation of neural circuits (Chen et al., 2014; Forrest et al., 2018; Isshiki et al., 2014; Penzes et al., 2011). Thereafter, the growth of excitatory synapses is gradually downregulated and unnecessary spines are selectively pruned, after which spines are maintained during adulthood. Time-lapse imaging experiments using *Auts2*-knocked-down hippocampal neurons revealed that *de novo* formation of dendritic spines is promoted, whereas the elimination rate is decreased, resulting in the exaggerated formation of excitatory synapses. These observations suggest an important role for AUTS2 in controlling the number of spines or excitatory synapses in forebrain neurons by modulating their turnover. We found that this excess in synapses was also observed in tamoxifen-treated *CaMKIIa-CreERT2;Auts2^{fllox/fllox}* in which *Auts2* was ablated after establishment of the brain structure. This suggests that AUTS2 is involved in regulating synaptic homeostasis at late developmental and/or adult stages.

Emerging evidence indicates that aberrant regulation of spine number and/or an increased excitatory synaptic inputs likely caused by incomplete pruning or exaggerated formation of spines is associated with numerous pathological conditions such as ASD, schizophrenia, and neurodegenerative disorders (Chen et al., 2014; Forrest et al., 2018; Lee et al., 2017; Penzes et al., 2011). Transcriptional control by epigenetic regulation including histone post-translational modification and chromatin remodeling is critical in synapse development and neurological disorders. A recent study by Korb et al. revealed that Fragile X mental retardation protein *Fmr1* mutant mice exhibit widespread histone mis-modifications (Korb et al., 2017). These are associated with open chromatin caused by upregulation of epigenetic factor Brd4, resulting in alteration of the transcription levels of many critical synapse-related genes. In this study, we showed that nuclear-localizing AUTS2 functions restrict spine number. Because AUTS2 is involved in transcriptional regulation via chromatin modification as a component of PRC1 (Gao et al., 2014), and because expression of many synapse-related genes was altered in the *Auts2* mutants (Figure 5), we believe that nuclear AUTS2 restricts the excitatory synapse number via controlling the expression of relevant genes, thus maintaining the excitation/inhibition balance of the brain.

In previous and current studies, we characterized behavioral phenotypes for two lines of mutant mice with different mutations disrupting the *Auts2* locus (Hori et al., 2015). We summarized the results from a behavioral test battery for *Auts2^{neo/+}* (Hori et al., 2015) and *Auts2^{delB/+}* mutant mice (this study) in

Figure S10D. In this study, we found that the *Auts2*^{del8/+} heterozygous global KO as well as *CaMKIIa-CreER*^{T2};*Auts2*^{fllox/fllox} conditional KO mice exhibited autistic-like behaviors including social deficits and altered vocal communications as well as multiple other behavioral impairments. In addition, *Auts2*^{del8/+} mice also showed altered anxiety as well as higher responses against nociceptive and auditory stimuli, both of which are often observed in patients with ASD (American Psychiatric Association, 2013). Interestingly, *Auts2*^{del8/+} mutant mice share several behavioral phenotypes with *Auts2*^{neo/+} mutants but also display a distinct combination of phenotypes (Figure S10D). Although the mechanisms underlying how different mutations lead to the distinct behavioral phenotypes in mice remains unclear, it is possible that compensatory expression of an AUTS2 C-terminal short isoform (S-AUTS2 var2) in *Auts2*^{del8/+} mutant brains negatively affects social behaviors in the social interaction tests (Figures 6A and 6B), whereas it alleviates the cognitive dysfunctions displayed in *Auts2*^{neo/+} mutant mice (Hori et al., 2015) such as the associative memory formation in fear-conditioning tests (Figure S10C). Alternatively, structural changes of the *Auts2* gene locus in these mutant mice could differentially impact on the expression of other AUTS2 isoforms, leading to the distinctive behavioral phenotypes, although we do not have a direct evidence of this. Further comparative analyses between these *Auts2* mutants will help us to understand the physiological function of AUTS2 in synapse development and the pathology of the AUTS2-related psychiatric illnesses.

In humans, it has been reported that multiple types of heterozygous genomic structural variants in the *AUTS2* locus including *de novo* balanced translocation, inversion, or intragenic deletions are associated with a wide range of psychiatric illnesses such as ASDs, ID, ADHD, schizophrenia, and dyslexia, as well as other neuropsychiatric diseases (Oksenberg and Ahituv, 2013). In addition to the exonic deletions of the *AUTS2* locus, some of the genomic structural variants are within non-coding regions including intronic and 5' upstream regions, implying that improper and disorganized expression of *AUTS2* could be involved in the onset of the disorders. However, it remains largely unclear how different mutations of the same gene contribute to different diseases. Currently, eight computationally annotated *AUTS2* isoforms in humans are incorporated in public databases (for example, the UCSC Genome Bioinformatics ([<https://genome.ucsc.edu>])). However, the study by Kondrychyn et al. revealed that *auts2a*, the zebrafish ortholog of *Auts2*, possesses 13 putative unique transcriptional start sites (TTS) and, surprisingly, more than 20 alternative transcripts are potentially produced from this gene locus by the aforementioned TSSs and/or by alternative splicing (Kondrychyn et al., 2017). These findings suggest that mammals including mouse and human could have similar or higher transcriptional complexity for *Auts2*/*AUTS2* than previously thought. Furthermore, Oksenberg et al. have identified several enhancer regions for the expression of *auts2a*/*Auts2* in zebrafish and mouse brain within the intronic regions of this gene locus (Oksenberg et al., 2013). Therefore, structural variants such as genomic deletions within a certain region of *Auts2*/*AUTS2* locus could not only alter the expression of full-length *AUTS2* directly but also affect the transcriptional regulation of other *AUTS2* isoforms. Different mutations of the *AUTS2* gene may differentially alter the temporal and spatial expression profiles of *AUTS2* isoforms in various brain regions, which may distinctively affect neurobiological functions, ultimately resulting in the occurrence of multiple types of psychiatric disorders in individuals with *AUTS2* syndrome. Our previous and this study, thus, highlighted that two types of *Auts2* mutants with different *AUTS2* protein expression profiles exhibited overlapping but distinct behavioral abnormalities. This may support the notion that different types of mutations in *AUTS2* account for distinct types of neuropsychiatric illnesses. Future comprehensive studies elucidating the regulatory mechanisms for transcription/splicing of *Auts2*/*AUTS2* as well as neurobiological functions of the distinctive *AUTS2* isoforms will help us to understand the pathogenic mechanisms underlying the occurrence of a variety of psychiatric disorders in individuals with *AUTS2* mutations and could contribute to therapeutic development for *AUTS2*-related neurological disorders.

In conclusion, the findings presented here suggest that synaptic regulation by *AUTS2* is required for proper social behaviors. Furthermore, our results from the behavioral analyses for *Auts2*^{del8/+} KO mice provided insight into the involvement of *AUTS2* in other higher brain functions such as recognition and emotion. In addition to the *AUTS2* function on synapse regulation, *AUTS2* is also involved in neuronal migration and neurite formation (Hori et al., 2014). Therefore, the other abnormal behaviors observed in *Auts2*^{del8/+} or *Auts2*^{neo/+} KO mice may partly be caused by the impairments in these developmental processes. Comparative analyses of the different forms of *Auts2* mouse mutants will help us to better understand the pathological mechanisms of the psychiatric disorders caused by *AUTS2* mutations. *Auts2* conditional KO mice

with *CaMKIIa-CreER^{T2}* or other more restricted-expression forms of *Cre* will be useful for dissecting the distinct neural circuitries involved in these abnormal behaviors.

Limitations of the Study

In this study, we demonstrated that the nuclear *AUTS2* controls the number of excitatory synapses in the forebrain pyramidal neurons, possibly by regulating the expression of genes for synapse development and functions. Transcriptome analysis revealed that loss of *Auts2* alters the expression levels of multiple synapse-related genes as well as genes for neuronal morphogenesis. The current study, however, does not address the mechanisms underlying the regulation of *AUTS2* in the expression of these synapse-related genes. Moreover, the *AUTS2* downstream targets that are responsible for dendritic spine development remains to be determined. Electrophysiological experiments reveal that increased dendritic spines caused by *Auts2* ablation in mice leads to the enhancement of excitatory synaptic inputs, resulting in a disturbed balance in excitatory and inhibitory synaptic inputs. We have not, however, evaluated the effects on synaptic plasticity such as long-term potentiation/depression. Further studies are required to address these issues to obtain a more complete picture of synaptic pathology caused by *AUTS2* mutations.

Resource Availability

Lead Contact

Further information and requests for resources should be directed to and will be fulfilled by the Lead Contact, Mikio Hoshino (hoshino@ncnp.go.jp).

Materials Availability

All unique materials generated from this study are available from the Lead Contact with a complete Materials Transfer Agreement.

Data and Code Availability

RNA-seq data have been deposited into GEO database with the accession number GSE134712.

METHODS

All methods can be found in the accompanying [Transparent Methods supplemental file](#).

SUPPLEMENTAL INFORMATION

Supplemental Information can be found online at <https://doi.org/10.1016/j.isci.2020.101183>.

ACKNOWLEDGMENTS

This work was supported by Grants-in-Aid for Scientific Research, KAKENHI (Grant 16H06528 and 18H02538 to M.H. and 16K07021 to K.H.), and Innovative Areas (16H06524 and 16H06531 to Y.G.) from MEXT; the SRPBS from AMED (JP19dm0107085), The Naito Foundation, Japan; Takeda Foundation, Japan; The Uehara Memorial Foundation, Japan; Suzuken Memorial Foundation, Japan; Princess Takamatsu Cancer Research Fund, Japan; and Intramural Research Grant (Grants 30-9 and 1-4 to M.H.). We are grateful to Dr. Ruth Yu (St Jude Children's Research Hospital) for comments on the manuscript.

AUTHOR CONTRIBUTIONS

K.H. designed this study. K.H. and M.H. wrote the manuscript and coordinated the project. K.H., Mitsuyo Yamada., S.F.E., K. Shimaoka., A.S., and M. Sone. performed and supervised imaging experiments and statistical analysis; W.S., T.N., and A.S. carried out and K. Yamada. supervised behavioral experiments and data analysis; K. Yamashiro., H. Kuniishi., K. Sohya., M. Sekiguchi., H. Kunugi., Mitsuhiro Yamada., and K.W. performed and supervised electrophysiological experiments; R.S. and K.K. performed and supervised recording and analysis of ultrasonic vocalizations; M.A. and K. Sakimura. generated and supervised the designs of *Auts2* mutant mice. Y.G., S.T., and S.M. performed RNA-seq and data analysis.

DECLARATION OF INTERESTS

The authors have declared that no conflict of interest exists.

Received: December 16, 2019

Revised: April 30, 2020

Accepted: May 15, 2020

Published: June 26, 2020

REFERENCES

- Amarillo, I.E., Li, W.L., Li, X., Vilain, E., and Kantarci, S. (2014). De novo single exon deletion of *AUTS2* in a patient with speech and language disorder: a review of disrupted *AUTS2* and further evidence for its role in neurodevelopmental disorders. *Am. J. Med. Genet. A* 164A, 958–965.
- American Psychiatric Association (2013). *Diagnostic and Statistical Manual of Mental Disorders, Fifth Edition* (American Psychiatric Association).
- Antoine, M.W., Langberg, T., Schnepel, P., and Feldman, D.E. (2019). Increased excitation-inhibition ratio stabilizes synapse and circuit excitability in four autism mouse models. *Neuron* 101, 648–661.e4.
- Bakkaloglu, B., O’Roak, B.J., Louvi, A., Gupta, A.R., Abelson, J.F., Morgan, T.M., Chawarska, K., Klin, A., Ercan-Sencicek, A.G., Stillman, A.A., et al. (2008). Molecular cytogenetic analysis and resequencing of contactin associated protein-like 2 in autism spectrum disorders. *Am. J. Hum. Genet.* 82, 165–173.
- Ballesteros-Yanez, I., Benavides-Piccione, R., Elston, G.N., Yuste, R., and DeFelipe, J. (2006). Density and morphology of dendritic spines in mouse neocortex. *Neuroscience* 138, 403–409.
- Bedogni, F., Hodge, R.D., Nelson, B.R., Frederick, E.A., Shiba, N., Daza, R.A., and Hevner, R.F. (2010). Autism susceptibility candidate 2 (*Auts2*) encodes a nuclear protein expressed in developing brain regions implicated in autism neuropathology. *Gene Expr. Patterns* 10, 9–15.
- Ben-David, E., Granot-Hershkovitz, E., Monderer-Rothkoff, G., Lerer, E., Levi, S., Yaari, M., Ebstein, R.P., Yirmiya, N., and Shifman, S. (2011). Identification of a functional rare variant in autism using genome-wide screen for monoallelic expression. *Hum. Mol. Genet.* 20, 3632–3641.
- Beunders, G., Voorhoeve, E., Golzio, C., Pardo, L.M., Rosenfeld, J.A., Talkowski, M.E., Simonin, I., Lionel, A.C., Vergult, S., Pyatt, R.E., et al. (2013). Exonic deletions in *AUTS2* cause a syndromic form of intellectual disability and suggest a critical role for the C terminus. *Am. J. Hum. Genet.* 92, 210–220.
- Bhatt, D.H., Zhang, S., and Gan, W.B. (2009). Dendritic spine dynamics. *Annu. Rev. Physiol.* 71, 261–282.
- Bourgeron, T. (2009). A synaptic trek to autism. *Curr. Opin. Neurobiol.* 19, 231–234.
- Chabout, J., Sarkar, A., Dunson, D.B., and Jarvis, E.D. (2015). Male mice song syntax depends on social contexts and influences female preferences. *Front. Behav. Neurosci.* 9, 76.
- Chao, H.T., Chen, H., Samaco, R.C., Xue, M., Chahrouh, M., Yoo, J., Neul, J.L., Gong, S., Lu, H.C., Heintz, N., et al. (2010). Dysfunction in GABA signaling mediates autism-like stereotypies and Rett syndrome phenotypes. *Nature* 468, 263–269.
- Chen, C.C., Lu, J., and Zuo, Y. (2014). Spatiotemporal dynamics of dendritic spines in the living brain. *Front. Neuroanat.* 8, 28.
- Davis, G.W. (2013). Homeostatic signaling and the stabilization of neural function. *Neuron* 80, 718–728.
- Edden, R.A., Crocetti, D., Zhu, H., Gilbert, D.L., and Mostofsky, S.H. (2012). Reduced GABA concentration in attention-deficit/hyperactivity disorder. *Arch. Gen. Psychiatry* 69, 750–753.
- Elia, J., Gai, X., Xie, H.M., Perin, J.C., Geiger, E., Glessner, J.T., D’Arcy, M., deBerardinis, R., Frackelton, E., Kim, C., et al. (2010). Rare structural variants found in attention-deficit hyperactivity disorder are preferentially associated with neurodevelopmental genes. *Mol. Psychiatry* 15, 637–646.
- Erdmann, G., Schutz, G., and Berger, S. (2007). Inducible gene inactivation in neurons of the adult mouse forebrain. *BMC Neurosci.* 8, 63.
- Fink, C.C., Bayer, K.U., Myers, J.W., Ferrell, J.E., Jr., Schulman, H., and Meyer, T. (2003). Selective regulation of neurite extension and synapse formation by the beta but not the alpha isoform of CaMKII. *Neuron* 39, 283–297.
- Forrest, M.P., Parnell, E., and Penzes, P. (2018). Dendritic structural plasticity and neuropsychiatric disease. *Nat. Rev. Neurosci.* 19, 215–234.
- Gangwar, S.P., Zhong, X., Seshadrinathan, S., Chen, H., Machius, M., and Rudenko, G. (2017). Molecular mechanism of *MDGA1*: regulation of neuroligin 2:neurexin trans-synaptic bridges. *Neuron* 94, 1132–1141.e4.
- Gao, Z., Lee, P., Stafford, J.M., von Schimmelmann, M., Schaefer, A., and Reinberg, D. (2014). An *AUTS2*-Polycomb complex activates gene expression in the CNS. *Nature* 516, 349–354.
- Gogolla, N., Leblanc, J.J., Quast, K.B., Sudhof, T.C., Fagiolini, M., and Hensch, T.K. (2009). Common circuit defect of excitatory-inhibitory balance in mouse models of autism. *J. Neurodev. Disord.* 1, 172–181.
- Han, S., Tai, C., Westenbroek, R.E., Yu, F.H., Cheah, C.S., Potter, G.B., Rubenstein, J.L., Scheuer, T., de la Iglesia, H.O., and Catterall, W.A. (2012). Autistic-like behaviour in *Scn1a*+/- mice and rescue by enhanced GABA-mediated neurotransmission. *Nature* 489, 385–390.
- Harper, K.M., Hiramoto, T., Tanigaki, K., Kang, G., Suzuki, G., Trimble, W., and Hiroi, N. (2012). Alterations of social interaction through genetic and environmental manipulation of the 22q11.2 gene *Sept5* in the mouse brain. *Hum. Mol. Genet.* 21, 3489–3499.
- Hiramoto, T., Kang, G., Suzuki, G., Satoh, Y., Kucherlapati, R., Watanabe, Y., and Hiroi, N. (2011). *Tbx1*: identification of a 22q11.2 gene as a risk factor for autism spectrum disorder in a mouse model. *Hum. Mol. Genet.* 20, 4775–4785.
- Holtmaat, A., and Svoboda, K. (2009). Experience-dependent structural synaptic plasticity in the mammalian brain. *Nat. Rev. Neurosci.* 10, 647–658.
- Holy, T.E., and Guo, Z. (2005). Ultrasonic songs of male mice. *PLoS Biol.* 3, e386.
- Hori, K., and Hoshino, M. (2017). Neuronal migration and *AUTS2* syndrome. *Brain Sci.* 7, 54.
- Hori, K., Nagai, T., Shan, W., Sakamoto, A., Abe, M., Yamazaki, M., Sakimura, K., Yamada, K., and Hoshino, M. (2015). Heterozygous disruption of autism susceptibility candidate 2 causes impaired emotional control and cognitive memory. *PLoS One* 10, e0145979.
- Hori, K., Nagai, T., Shan, W., Sakamoto, A., Taya, S., Hashimoto, R., Hayashi, T., Abe, M., Yamazaki, M., Nakao, K., et al. (2014). Cytoskeletal regulation by *AUTS2* in neuronal migration and neurogenesis. *Cell Rep.* 9, 2166–2179.
- Hutsler, J.J., and Zhang, H. (2010). Increased dendritic spine densities on cortical projection neurons in autism spectrum disorders. *Brain Res.* 1309, 83–94.
- Isshiki, M., Tanaka, S., Kuriu, T., Tabuchi, K., Takumi, T., and Okabe, S. (2014). Enhanced synapse remodelling as a common phenotype in mouse models of autism. *Nat. Commun.* 5, 4742.
- Iwasato, T., Datwani, A., Wolf, A.M., Nishiyama, H., Taguchi, Y., Tonegawa, S., Knopfel, T., Erzurumlu, R.S., and Itoharu, S. (2000). Cortex-restricted disruption of *NMDAR1* impairs neuronal patterns in the barrel cortex. *Nature* 406, 726–731.
- Jolley, A., Corbett, M., McGregor, L., Waters, W., Brown, S., Nicholl, J., and Yu, S. (2013). De novo intragenic deletion of the autism susceptibility candidate 2 (*AUTS2*) gene in a patient with developmental delay: a case report and literature review. *Am. J. Med. Genet. A* 161A, 1508–1512.
- Kalscheuer, V.M., FitzPatrick, D., Tommerup, N., Bugge, M., Niebuhr, E., Neumann, L.M., Tzschach, A., Shoichet, S.A., Menzel, C., Erdogan, F., et al. (2007). Mutations in autism susceptibility candidate 2 (*AUTS2*) in patients with mental retardation. *Hum. Genet.* 121, 501–509.
- Kondrychyn, I., Robra, L., and Thirumalai, V. (2017). Transcriptional complexity and distinct expression patterns of *auts2* paralogs in *Danio rerio*. *G3 (Bethesda)* 7, 2577–2593.

- Korb, E., Herre, M., Zucker-Scharff, I., Gresack, J., Allis, C.D., and Darnell, R.B. (2017). Excess translation of epigenetic regulators contributes to fragile X syndrome and is alleviated by Brd4 inhibition. *Cell* 170, 1209–1223.e20.
- Lee, E., Lee, J., and Kim, E. (2017). Excitation/inhibition imbalance in animal models of autism spectrum disorders. *Biol. Psychiatry* 81, 838–847.
- Luhmann, H.J., Huston, J.P., and Hasenohrl, R.U. (2005). Contralateral increase in thigmotactic scanning following unilateral barrel-cortex lesion in mice. *Behav. Brain Res.* 157, 39–43.
- Martinelli, D.C., Chew, K.S., Rohlmann, A., Lum, M.Y., Ressler, S., Hattar, S., Brunger, A.T., Missler, M., and Sudhof, T.C. (2016). Expression of C1q3 in discrete neuronal populations controls efferent synapse numbers and diverse behaviors. *Neuron* 91, 1034–1051.
- Matsuda, K., Budisantoso, T., Mitakidis, N., Sugaya, Y., Miura, E., Kakegawa, W., Yamasaki, M., Konno, K., Uchigashima, M., Abe, M., et al. (2016). Transsynaptic modulation of kainate receptor functions by C1q-like proteins. *Neuron* 90, 752–767.
- Milani, H., Steiner, H., and Huston, J.P. (1989). Analysis of recovery from behavioral asymmetries induced by unilateral removal of vibrissae in the rat. *Behav. Neurosci.* 103, 1067–1074.
- Monderer-Rothkoff, G., Tal, N., Risman, M., Shani, O., Nissim-Rafinia, M., Malki-Feldman, L., Medvedeva, V., Groszer, M., Meshorer, E., and Shifman, S. (2019). AUTS2 isoforms control neuronal differentiation. *Mol. Psychiatry*. <https://doi.org/10.1038/s41380-019-0409-1>.
- Moosmang, S., Haider, N., Klugbauer, N., Adelsberger, H., Langwieser, N., Muller, J., Stiess, M., Marais, E., Schulla, V., Lacinova, L., et al. (2005). Role of hippocampal Cav1.2 Ca²⁺ channels in NMDA receptor-independent synaptic plasticity and spatial memory. *J. Neurosci.* 25, 9883–9892.
- Oksenberg, N., and Ahituv, N. (2013). The role of AUTS2 in neurodevelopment and human evolution. *Trends Genet.* 29, 600–608.
- Oksenberg, N., Stevison, L., Wall, J.D., and Ahituv, N. (2013). Function and regulation of AUTS2, a gene implicated in autism and human evolution. *PLoS Genet.* 9, e1003221.
- Penzes, P., Cahill, M.E., Jones, K.A., VanLeeuwen, J.E., and Woolfrey, K.M. (2011). Dendritic spine pathology in neuropsychiatric disorders. *Nat. Neurosci.* 14, 285–293.
- Pettem, K.L., Yokomaku, D., Takahashi, H., Ge, Y., and Craig, A.M. (2013). Interaction between autism-linked MDGAs and neurologins suppresses inhibitory synapse development. *J. Cell Biol.* 200, 321–336.
- Portfors, C.V., and Perkel, D.J. (2014). The role of ultrasonic vocalizations in mouse communication. *Curr. Opin. Neurobiol.* 28, 115–120.
- Ramocki, M.B., and Zoghbi, H.Y. (2008). Failure of neuronal homeostasis results in common neuropsychiatric phenotypes. *Nature* 455, 912–918.
- Rubenstein, J.L., and Merzenich, M.M. (2003). Model of autism: increased ratio of excitation/inhibition in key neural systems. *Genes Brain Behav.* 2, 255–267.
- Sagar, S.M., Sharp, F.R., and Curran, T. (1988). Expression of c-fos protein in brain: metabolic mapping at the cellular level. *Science* 240, 1328–1331.
- Sultana, R., Yu, C.E., Yu, J., Munson, J., Chen, D., Hua, W., Estes, A., Cortes, F., de la Barra, F., Yu, D., et al. (2002). Identification of a novel gene on chromosome 7q11.2 interrupted by a translocation breakpoint in a pair of autistic twins. *Genomics* 80, 129–134.
- Takahashi, T., Okabe, S., Broin, P.O., Nishi, A., Ye, K., Beckert, M.V., Izumi, T., Machida, A., Kang, G., Abe, S., et al. (2016). Structure and function of neonatal social communication in a genetic mouse model of autism. *Mol. Psychiatry* 21, 1208–1214.
- Talkowski, M.E., Rosenfeld, J.A., Blumenthal, I., Pillalamarri, V., Chiang, C., Heilbut, A., Ernst, C., Hanscom, C., Rossin, E., Lindgren, A.M., et al. (2012). Sequencing chromosomal abnormalities reveals neurodevelopmental loci that confer risk across diagnostic boundaries. *Cell* 149, 525–537.
- Tang, G., Gudsnuk, K., Kuo, S.H., Cotrina, M.L., Rosoklija, G., Sosunov, A., Sonders, M.S., Kanter, E., Castagna, C., Yamamoto, A., et al. (2014). Loss of mTOR-dependent macroautophagy causes autistic-like synaptic pruning deficits. *Neuron* 83, 1131–1143.
- Tien, N.W., and Kerschensteiner, D. (2018). Homeostatic plasticity in neural development. *Neural Dev.* 13, 9.
- van Woerden, G.M., Hoebeek, F.E., Gao, Z., Nagaraja, R.Y., Hoogenraad, C.C., Kushner, S.A., Hansel, C., De Zeeuw, C.I., and Elgersma, Y. (2009). betaCaMKII controls the direction of plasticity at parallel fiber-Purkinje cell synapses. *Nat. Neurosci.* 12, 823–825.
- Wasser, C.R., and Herz, J. (2017). Reelin: neurodevelopmental architect and homeostatic regulator of excitatory synapses. *J. Biol. Chem.* 292, 13330–13338.
- Wefelmeyer, W., Puhl, C.J., and Burrone, J. (2016). Homeostatic plasticity of subcellular neuronal structures: from inputs to outputs. *Trends Neurosci.* 39, 656–667.
- Zhang, B., Xu, Y.H., Wei, S.G., Zhang, H.B., Fu, D.K., Feng, Z.F., Guan, F.L., Zhu, Y.S., and Li, S.B. (2014). Association study identifying a new susceptibility gene (AUTS2) for schizophrenia. *Int. J. Mol. Sci.* 15, 19406–19416.

Supplemental Information

AUTS2 Regulation of Synapses for Proper Synaptic Inputs and Social Communication

Kei Hori, Kunihiro Yamashiro, Taku Nagai, Wei Shan, Saki F. Egusa, Kazumi Shimaoka, Hiroshi Kuniishi, Masayuki Sekiguchi, Yasuhiro Go, Shoji Tatsumoto, Mitsuyo Yamada, Reika Shiraishi, Kouta Kanno, Satoshi Miyashita, Asami Sakamoto, Manabu Abe, Kenji Sakimura, Masaki Sone, Kazuhiro Sohya, Hiroshi Kunugi, Keiji Wada, Mitsuhiko Yamada, Kiyofumi Yamada, and Mikio Hoshino

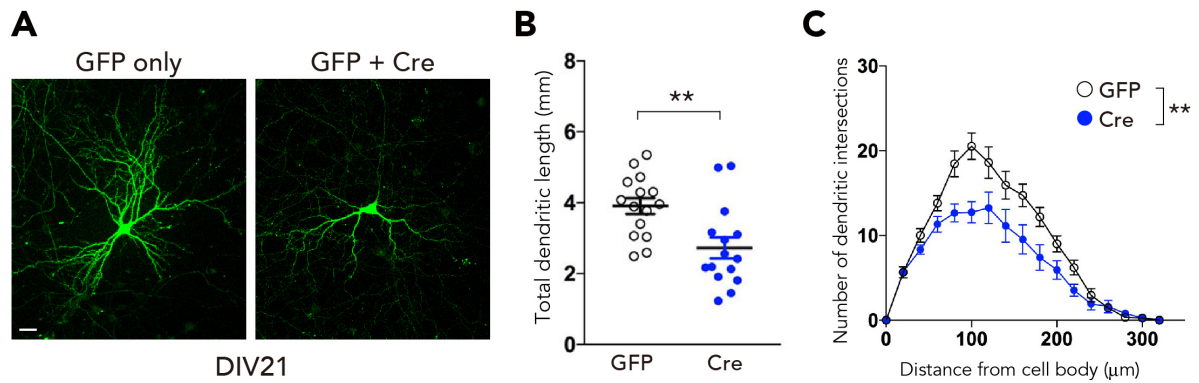


Figure S1. *Auts2* mutant primary hippocampal neurons exhibit the impairment of dendritic morphogenesis, Related to Figure 1.

(A) Representative images of cultured primary hippocampal control (GFP only) and *Auts2*-deficient neurons (GFP + Cre) at DIV21. Neurons derived from *Auts2*^{flax/flax} homozygotic brains were electroporated with control or Cre expression vectors at DIV0. GFP expression vector was co-electroporated to visualize the neurons. (B) Measurement of total dendritic length (n = 15 neurons). (C) Sholl analysis. Graph shows the number of dendritic intersections of dendrites per each Sholl ring (20 μm interval concentric circles centered on the soma) for the control (GFP only) and *Auts2*-deficient (GFP + Cre) neurons at DIV21 (n=15 neurons). Data are mean \pm SEM. ** $P < 0.01$. (B) unpaired t-test, (C) repeated-measure ANOVA. Scale bar, 20 μm .

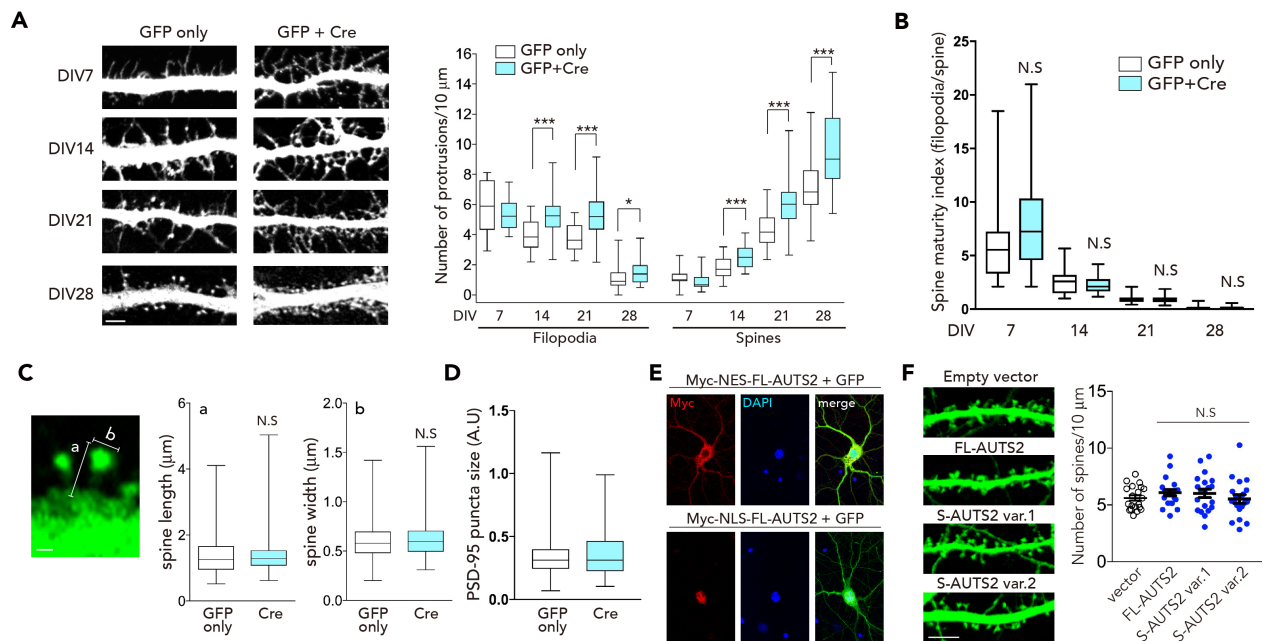


Figure S2. *Auts2* mutant primary neurons exhibit excessive spine formation, Related to Figure 1.

(A) The representative images of secondary dendritic segments of cultured primary hippocampal neurons. The neurons derived from *Auts2*^{fllox/fllox} homozygotes were electroporated with the control or Cre expression vectors. To visualize the neurons, GFP expression vector was co-electroporated. The density of dendritic spines and filopodia on the dendrites of the control and *Auts2* KO (Cre) neurons were measured at different culture stages (DIV7-28) (n=21-40 dendrites of 11-20 neurons). (B) Graph shows the spine maturity index defined by the ratio of filopodia to mushroom spine. (C) The length of dendritic spines (a) and width of the spine head (b) in the control (GFP only) and *Auts2* KO neurons (Cre) at DIV28 were measured (control; n=155 spines, Cre; n=158 spines). (D) The measurement of PSD-95 puncta size in control (GFP only) and *Auts2* KO neurons (Cre) at DIV 21 (n=160). A.U, arbitrary unit. (E) Subcellular localization of Myc-NES- and Myc-NLS-FL-AUTS2^R in WT primary hippocampal neurons at DIV12. (F) WT primary hippocampal neurons were co-electroporated with GFP and expression vectors for the full-length AUTS2 (FL-AUTS2) and C-terminal AUTS2 short variants (S-AUTS2 var.1 and var.2) or control plasmid (Empty vector). The density of dendritic spines was measured at DIV24 (n = 20 dendrites). Data are mean ± SEM and box-and-whisker plots (medians with interquartile range, minimum, and maximum values are represented). *P < 0.05, ***P < 0.001, N.S, not significant. (A and C) unpaired t-test, (B and D) Mann-Whitney U test, (F) one-way ANOVA with Dunnett's post hoc test. Quantifications represent data from three independent experiments. Scale bar, 5 μm in (A, E and G) and 1 μm in (C).

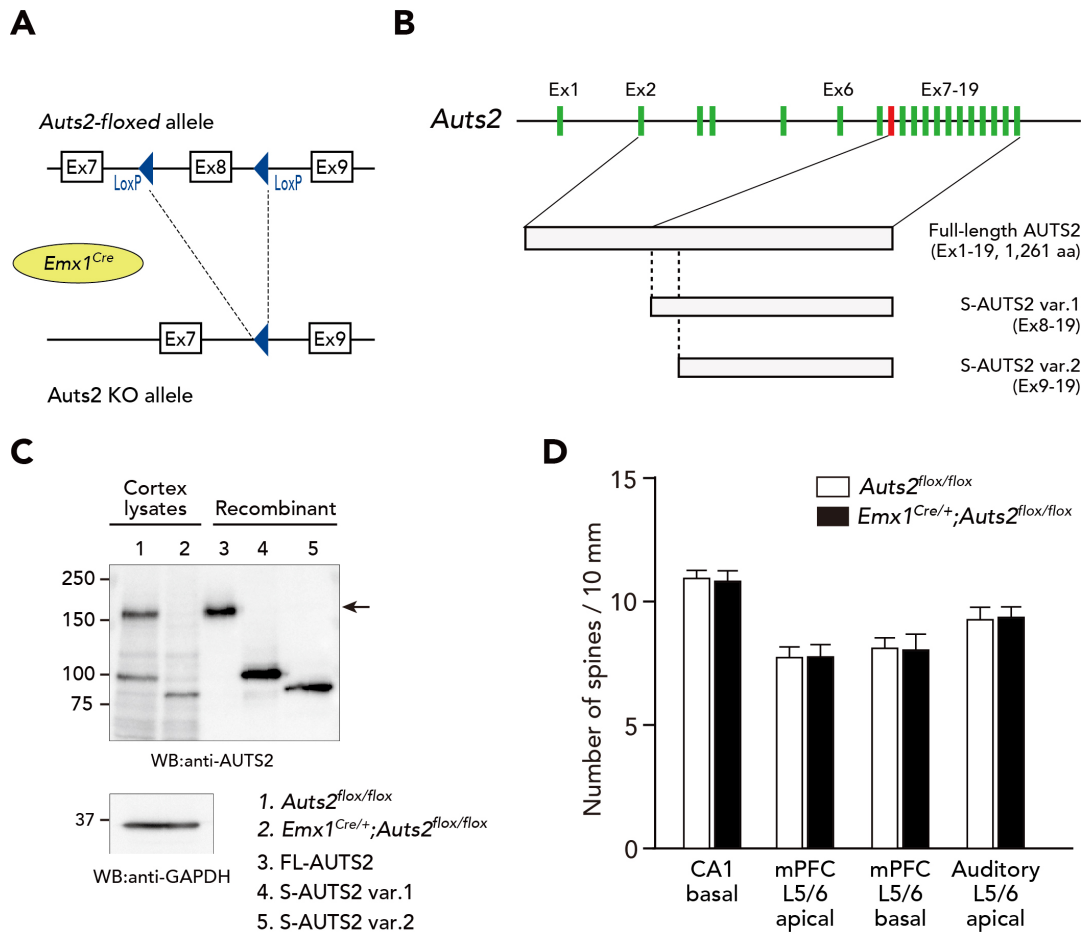


Figure S3. Analysis of spine formation in forebrain-specific *Aut2* conditional KO mice, Related to Figure 2.

(A) Schematics of the targeting strategy. The deletion of exon 8 at *Aut2* locus in pyramidal neurons of the forebrain was generated by crossing the *Aut2*-floxed mice with *Emx1^{Cre}* mice. (B) Schematic of *Aut2* genomic region and the protein structure of AUTS2 isoforms. (C) Western blotting of lysates from P0 cerebral cortex of *Aut2^{flox/flox}* (Control) and *Emx1^{Cre/+};Aut2^{flox/flox}* homozygotes using anti-AUTS2 antibody. Immunoblot of lysates from HEK293T cells expressing the recombinant full-length AUTS2 and the C-terminal AUTS2 short variants (S-AUTS2 var.1 and var.2) are also shown. Full-length AUTS2 (arrow) as well as the S-AUTS2 var.1 were completely eliminated in *Aut2* homozygotic mutant cerebral cortices whereas the S-AUTS2 var.2 was alternatively increased. (D) Summary graph of the spine density on the basal dendrites of CA1 pyramidal neurons, apical and basal dendrites of the deep-layer (L5/6) neurons at mPFC and auditory cortex in the *Aut2^{flox/flox}* and *Emx1^{Cre/+};Aut2^{flox/flox}* homozygotic mutant mouse brains. (n=20 dendrites from N=3 animals) Data are presented as mean \pm SEM. unpaired t-test. Scale bar, 10 μ m.

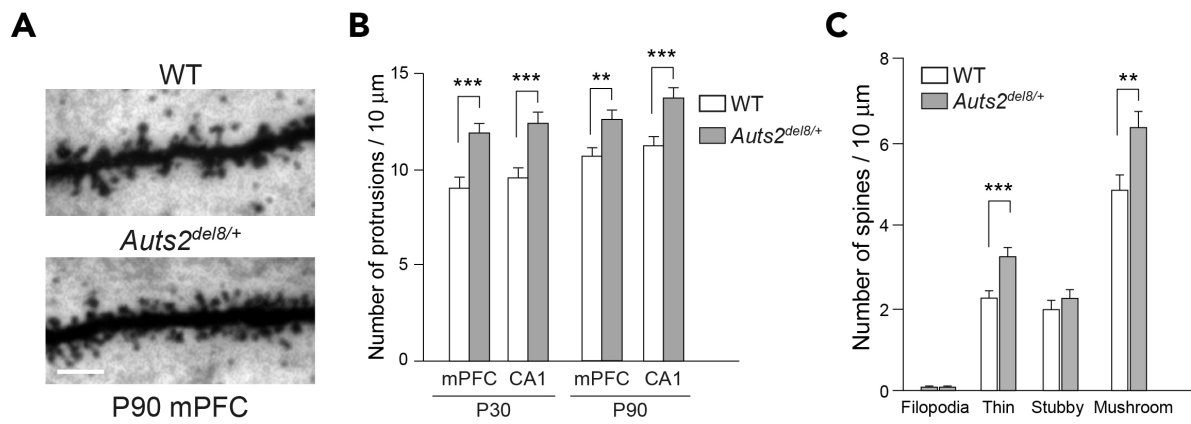


Figure S4. Spines were abnormally increased in the constitutive *AutS2^{del8/+}* mutant mature brains *in vivo*, Related to Figure 2.

(A) Representative images of the dendritic spines from Golgi-stained upper-layer pyramidal neurons in the mPFC of WT (upper panel) and *AutS2^{del8/+}* heterozygotic mutant mouse brains (lower panel) at P90. (B) Summary graph of the spine density on the neurons in indicated brain areas in WT and *AutS2^{del8/+}* heterozygotes at young adult (P30) and mature adult (P90). (n=20 dendrites from n=3 animals). (C) The density of each category of spines in the upper-layer neurons in the mPFC was measured in WT and *AutS2^{del8/+}* mutant mouse brains at P90 (n=20 dendrites from n=3 animals). Data are presented as mean \pm SEM. ** $P < 0.01$, *** $P < 0.001$, (B) unpaired t-test, (C) Mann-Whitney U test. Scale bar, 5 μm .

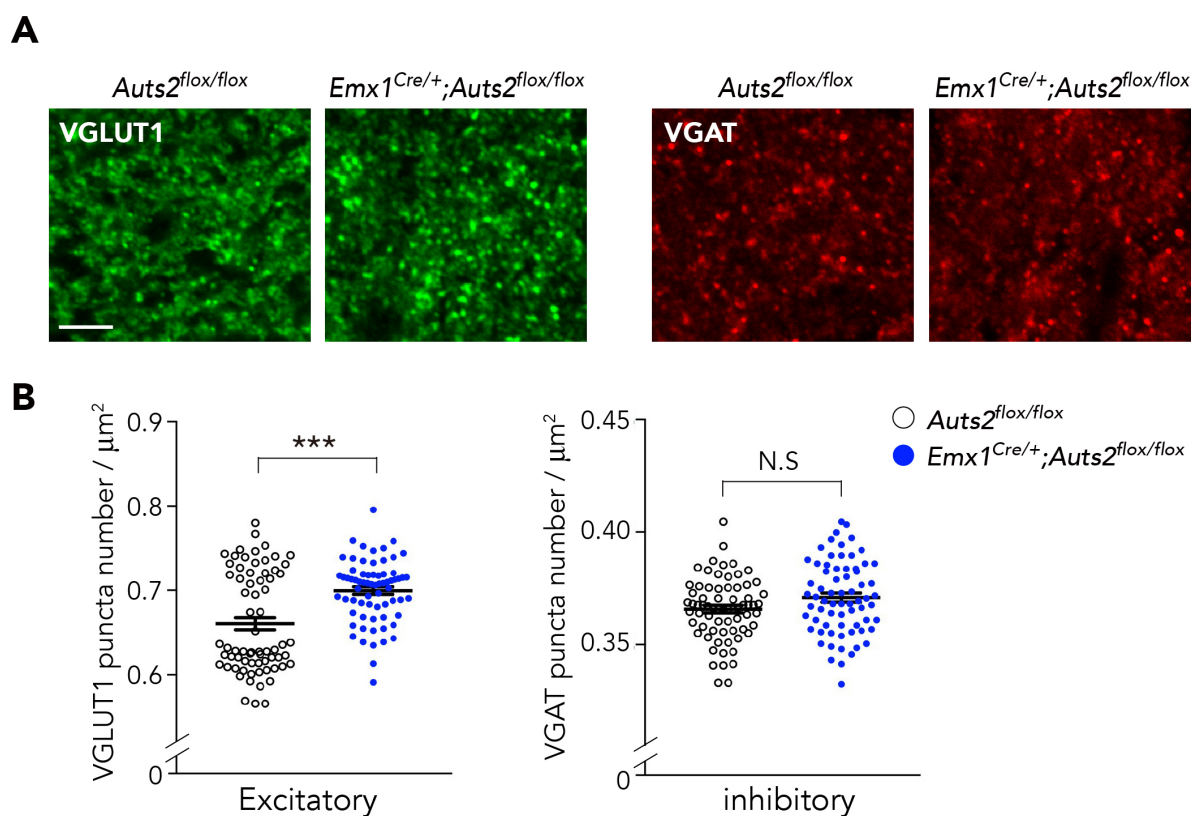


Figure S5. Loss of *Auts2* in the forebrain induces the aberrant excitatory synapse formation, Related to Figure 2.

(A) Representative images of upper-layer in medial prefrontal cortex (mPFC) sections from *Auts2* homozygotic mutant (*Emx1^{Cre/+};Auts2^{flox/flox}*) and control (*Auts2^{flox/flox}*) mice at P35 stained with VGLUT1 (green) or VGAT (red), for excitatory and inhibitory presynaptic markers, respectively. (B) Quantification of the density of VGLUT1- and VGAT-positive synaptic puncta in the mPFC. Data are means \pm SEM ($n = 69$ sections from $N = 3$ brains). $**P < 0.001$, N.S, not significant. (B) Mann-Whitney U test. Scale bar, $5 \mu\text{m}$.

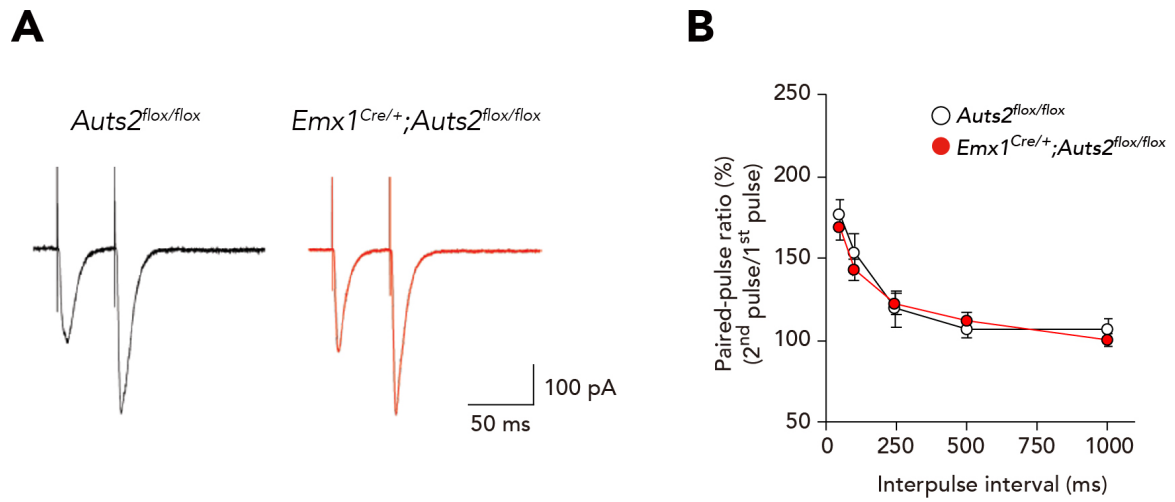


Figure 6. Electrophysiological analysis of CA1 pyramidal neurons in *Emx1^{Cre};Auts2^{flox}* mutant mice, Related to Figure 3.

(A) Representative traces showing evoked EPSCs in response to paired sets of local stimulation at Schaffer collaterals in CA1 hippocampal region. (B) Plot of the paired-pulse ratio (interpulse interval: 50 ms, 100 ms, 250 ms, 500 ms and 1000 ms), calculated as the ratio (%) of the second to first EPSC amplitude (n=12 cells from 3-4 mice). Data are mean ± SEM. (B) repeated-measure ANOVA.

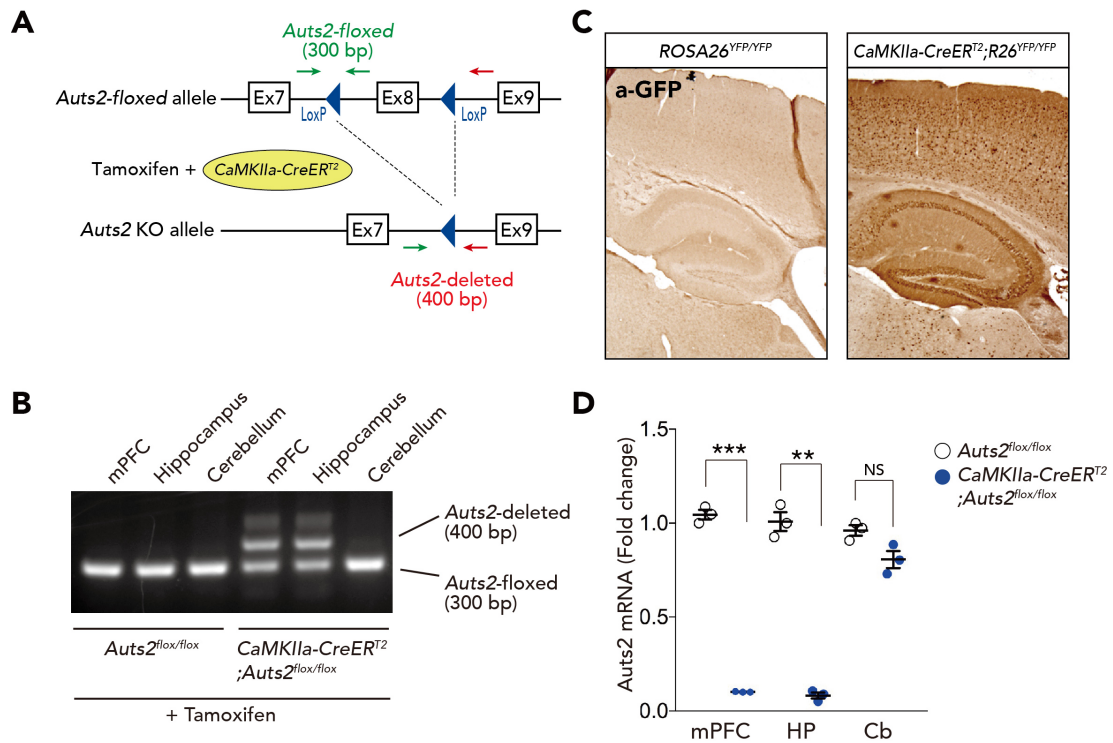


Figure S7. Conditional deletion of *Aut2* in postnatal forebrain leads to excessive spine formation, Related to Figure 4.

(A) Schematics of the targeting strategy. The inducible conditional deletion of exon 8 at *Aut2* locus in pyramidal neurons of the forebrain was generated by breeding the *Aut2*^{fl/ox/fl/ox} mice to *CaMKIIa-CreER*^{T2} mice. (B) The forebrain-specific deletion of *Aut2* locus in the homozygous mutants (*CaMKIIa-CreER*^{T2}; *Aut2*^{fl/ox/fl/ox}) and control littermates (*Aut2*^{fl/ox/fl/ox}) after tamoxifen administration was confirmed by genomic PCR using the primer pairs indicated as green and red arrows in (A). (C) Examination of *CreER*^{T2} recombinase activity in the postnatal brain. Tamoxifen was administered to *CaMKIIa-CreER*^{T2}; *ROSA26R*^{YFP/YFP} reporter mice and the *ROSA26R*^{YFP/YFP} control littermate during P21-25. Brain sections isolated 10 days after tamoxifen treatment were DAB-stained with anti-GFP antibody. The expression of EYFP was observed in the cortex and hippocampus in the presence of the *CreER*^{T2} transgene (right panel). (D) Examination of *Aut2* transcript levels in mPFC, hippocampus (HP) and cerebellum (Cb) of adult *CaMKIIa-CreER*^{T2}; *Aut2*^{fl/ox/fl/ox} homozygotic mutant mice and the control mice (*Aut2*^{fl/ox/fl/ox}) with tamoxifen application. qPCR was performed using primers specific for the deleted exon (n=3 brains). Data are mean ± SEM. ***P* < 0.01, ****P* < 0.001, unpaired t-test. Scale bar, 10 μm.

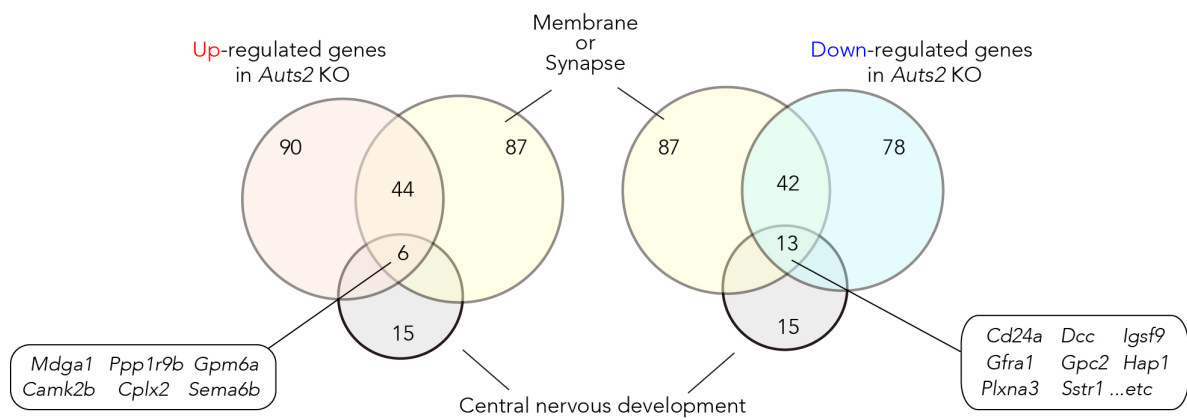


Figure S8. Transcriptome analysis of *Emx1^{Cre/+};Aut2^{flox/flox}* mutant mice hippocampal brain tissues, Related to Figure 5.

Venn diagram showing the number of up-regulated or down-regulated genes in *Aut2* KO categorized in "membrane" (GO:0016020) or "synapse" (GO:0045202) and "central nervous development" (GO:0007399).

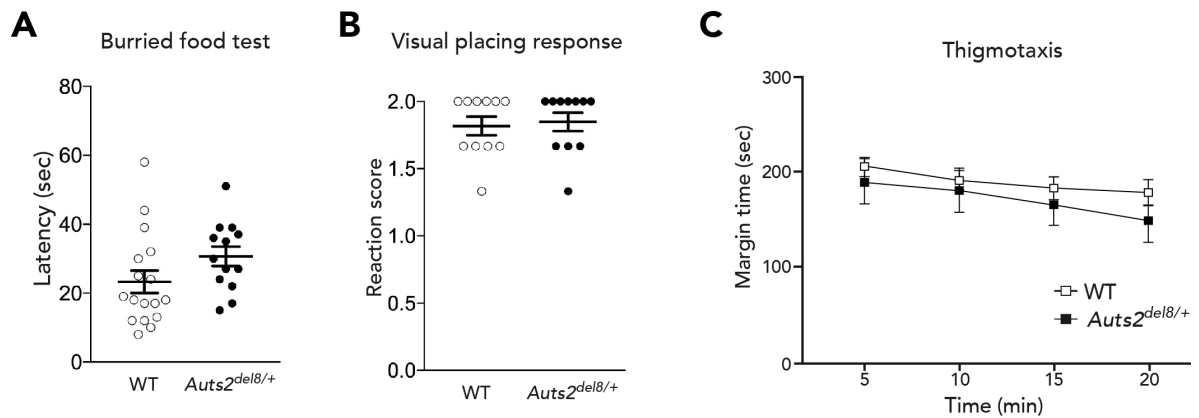


Figure S9. *Aut2^{del8/+}* mutant mice exhibit normal sensory abilities, Related to Figure 6.

(A) The buried food finding test. Time spent to find buried food pellet was measured. (WT, n=17, *Aut2^{del8/+}* n=13). (B) Visual placing response test. Reaction score was rated as follow: 0, no observable placing behavior; 1, a weak or delayed placing response; 2, a clear placing reaction. (WT, n=11, *Aut2^{del8/+}* n=11). (C) Thigmotaxis. Time spent in the margin area of the open field box was measured every 5 min for 20 min. (WT, n=10, *Aut2^{del8/+}* n=10). Data are mean \pm SEM. (A and B) Mann-Whitney U test, (C) two-way ANOVA with repeated measures.

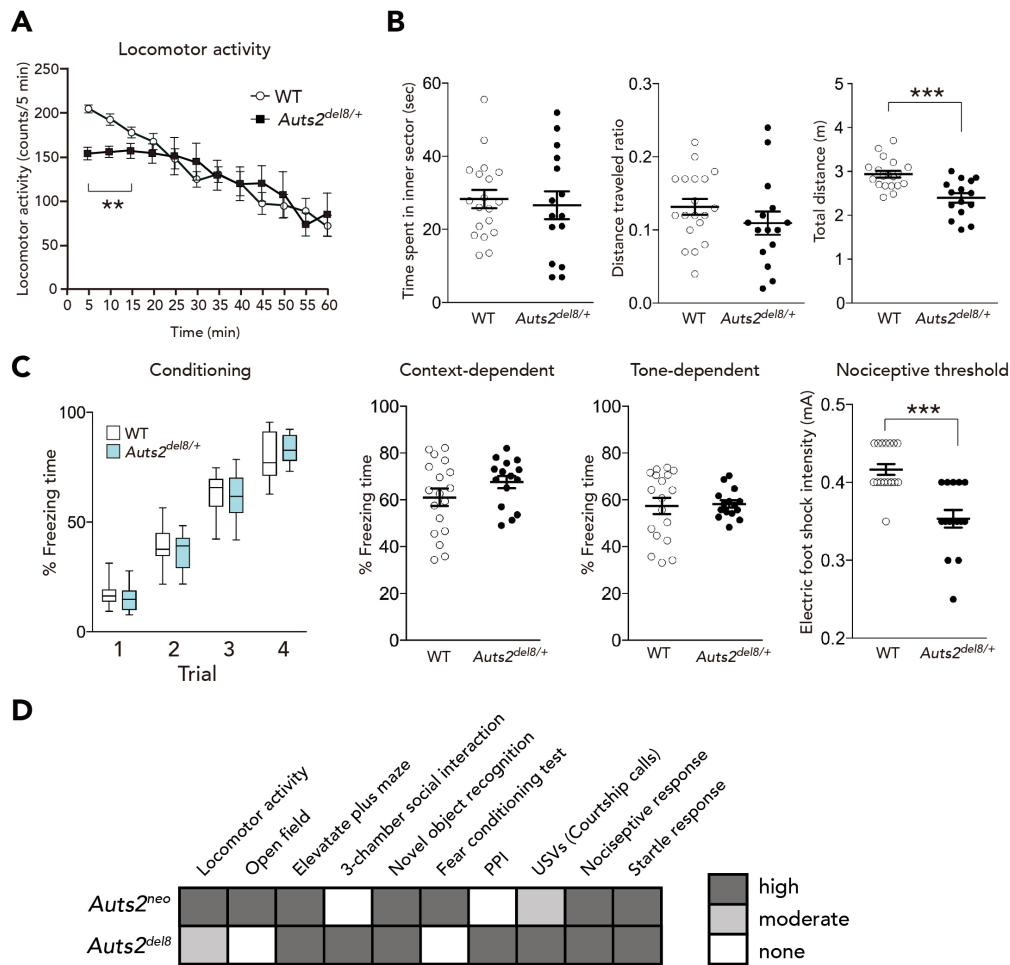


Figure S10. Behavioral analyses of *Auts2*^{delB/+} mutant mice, Related to Figure 6.

(A) Spontaneous locomotor activity of mice in a novel environment was measured every 5 min for 60 min. *Auts2*^{delB/+} mutant mice displayed a decrease in exploratory behavior during the first 15 min period (WT, n=19, *Auts2*^{delB/+}, n=16). (B) In open field tests, *Auts2*^{delB/+} mutant mice exhibited a decrease in total distance traveled in a test field area for 5 min (right graph) whereas there was no significant difference between genotypes in time spent in an inner area (left graph) as well as the ratio of distance traveled in an inner area scored as the percentage of total distance traveled (middle graph) (WT, n=19, *Auts2*^{delB/+}, n=15). (C) Associative memory of WT and *Auts2*^{delB/+} mutant mice was measured by the contextual (Context-dependent) and tone cued (Tone-dependent) fear-conditioning test 24 hrs after the conditioning phase (Conditioning). Freezing responses of *Auts2*^{delB/+} mice during contextual and cued memory test were comparable to WT mice while *Auts2* mutant mice exhibited a higher response to lower nociceptive stimuli relative to WT mice (Nociceptive threshold) (WT, n=18, *Auts2*^{delB/+}, n=15). (D) Summary of the results from behavioral test battery for *Auts2*^{neo/+} (Hori et al., 2015) and *Auts2*^{delB/+} mutant mice. Data are mean ± SEM and box-and-whisker plots (medians with interquartile range, minimum, and maximum values are represented). ***P* < 0.01, ****P* < 0.001, (A) two-way ANOVA with repeated measures, (B) unpaired t-test, (C) two-way ANOVA with repeated measures in conditioning and Mann-Whitney U test in freezing responses.

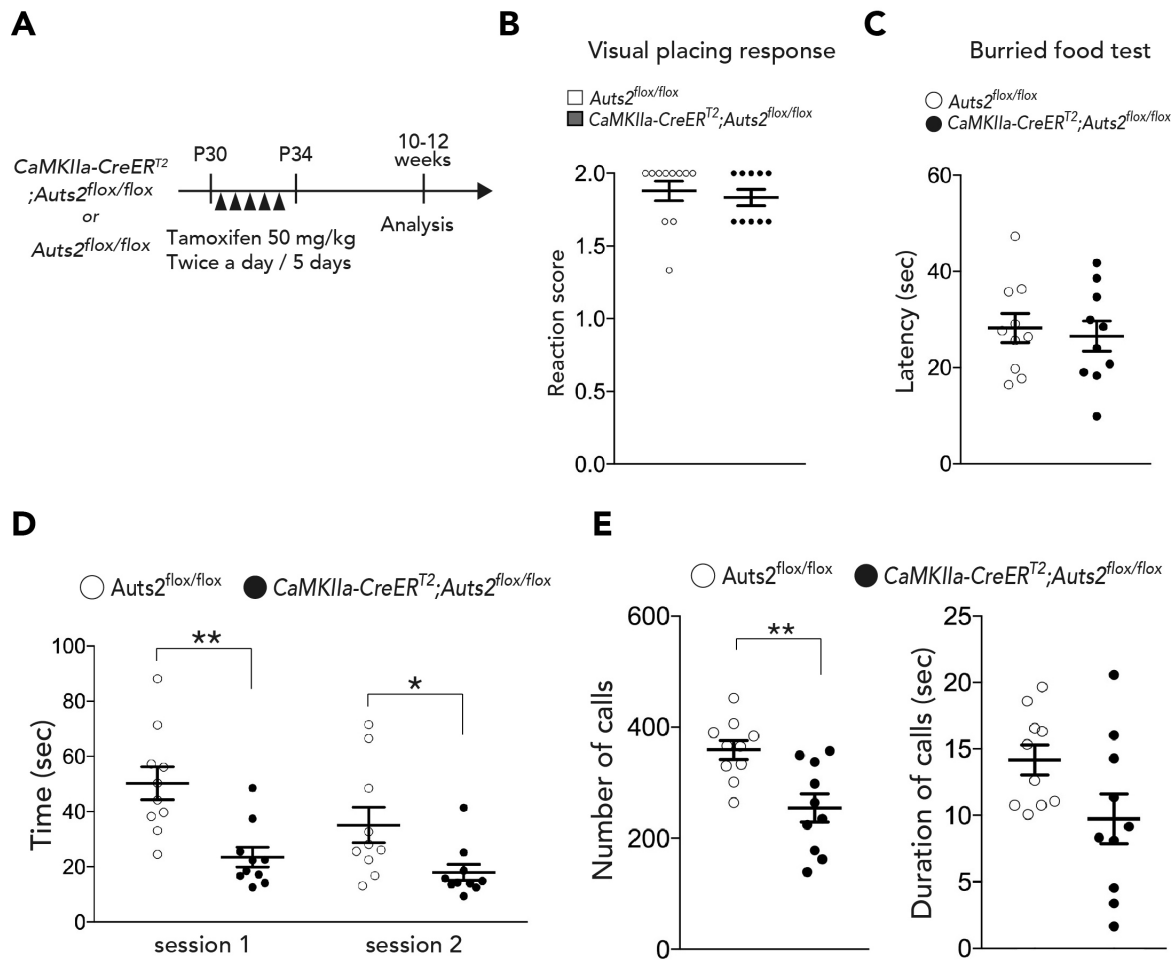


Figure S11. Behavioral analyses of *CaMKIIa-CreER^{T2};Auts2^{flox/flox}* mice, Related to Figure 6 and 7.

(A) Scheme illustrating the tamoxifen-inducible deletion of *Auts2* in postnatal forebrain. Tamoxifen was administered to *CaMKIIa-CreER^{T2};Auts2^{flox/flox}* homozygotes and their control *Auts2^{flox/flox}* littermate mice during P30-34 and behavioral analyses were performed during 10-12 weeks. (B) Visual placing response test. Reaction score was rated as follow: 0, no observable placing behavior; 1, a weak or delayed placing response; 2, a clear placing reaction. (*Auts2^{flox/flox}*, n=11, *CaMKIIa-CreER^{T2};Auts2^{flox/flox}* n=10). (C) The buried food finding test. Time spent to find buried food pellet was measured. (*Auts2^{flox/flox}*, n=10, *CaMKIIa-CreER^{T2};Auts2^{flox/flox}*, n=10). (D) Reciprocal social interaction test. Social interaction between *Auts2^{flox/flox}* or *CaMKIIa-CreER^{T2};Auts2^{flox/flox}* mouse pairs during 5 min were measured (*Auts2^{flox/flox}*, n=10, *CaMKIIa-CreER^{T2};Auts2^{flox/flox}* n=10). (E) The number (left) and duration (right) of USVs during 1 min in adult *Auts2^{flox/flox}* or *CaMKIIa-CreER^{T2};Auts2^{flox/flox}* mice (*Auts2^{flox/flox}*, n=10, *CaMKIIa-CreER^{T2};Auts2^{flox/flox}* n=10). Data are the means \pm SEM. * $P < 0.05$, ** $P < 0.01$, (B ,C and E) unpaired t-test, (D) two-way ANOVA.

Mouse strain	Allele type	Genotype
<i>Auts2^{neo}</i>	Global KO (Neo gene knock-in)	WT (Control) <i>Auts2^{Neo/+}</i> (Heterozygote)
<i>Auts2^{del8}</i>	Global KO (Exon 8 deleted)	WT (Control) <i>Auts2^{del8/+}</i> (Heterozygote)
<i>Emx1^{Cre};Auts2^{flox}</i>	forebrain-specific conditional KO (Exon 8 deleted)	<i>Auts2^{flox/flox}</i> (Control) <i>Emx1^{Cre/+};Auts2^{flox/+}</i> (Heterozygote) <i>Emx1^{Cre/+};Auts2^{flox/flox}</i> (Homozygote)
<i>CaMKIIa-CreER^{T2};Auts2^{flox}</i>	Tamoxifen-inducible mature projection neuron -specific conditional KO (Exon 8 deleted)	<i>Auts2^{flox/flox}</i> (Control) <i>CaMKIIa-CreER^{T2};Auts2^{flox/flox}</i> (Homozygote)

Table S1. Summary of *Auts2* mutant mouse strains, Related to Figure 2, 4, 6 and 7.

Transparent Methods

Experimental animals

Rosa26^{YFP} mouse line (stock no. 006148) was obtained from The Jackson Laboratory. Genotyping for the *Auts2*-floxed mice with a pure C57BL/6N genetic background was performed by PCR with the following primers: (F) 5'-GGCAGGTGGTTAGGTTACA-3'; (R) 5'-CAGTGCTAGAATCACAGCTG-3'. For *Auts2^{del8}* mice with C57BL/6N background, the following genotyping primer was used with the above two primers: 5'-ATCTTGGGTCCTTCCTCAG-3' (Table S1) (Hori et al., 2014). *Emx1^{Cre}* (stock #RBRC00808, C57BL/6J background) and *CaMKIIa-CreER^{T2}* (B6.FVB-Tg(Camk2a-cre/ERT2)2Gsc/leg, stock #EM02125) mice were purchased from RIKEN BioResource Center (RIKEN, Tsukuba, Japan) and European Mouse Mutant Archive (EMMA) (HelmholtzZentrum München, Neuherberg, Germany), respectively (Erdmann et al., 2007; Iwasato et al., 2000). *Emx1^{Cre}* mice were backcrossed for 8 generations to C57BL/6N wild type mice (Charles River Laboratories, Kanagawa, Japan) before crossing with *Auts2^{flox/flox}* mice. *Emx1^{Cre/+};Auts2^{flox/flox}* homozygous mutant mice were generated by crossing *Emx1^{Cre/+}* mice with *Auts2^{flox/flox}* mice to yield *Emx1^{Cre/+};Auts2^{flox/+}* heterozygous mutant progeny. *Emx1^{Cre/+};Auts2^{flox/+}* male mice were then crossed with *Auts2^{flox/flox}* female mice to obtain litters consisting of control (*Auts2^{flox/+}* or *Auts2^{flox/flox}*) mice, heterozygous (*Emx1^{Cre/+};Auts2^{flox/+}*) or homozygous (*Emx1^{Cre/+};Auts2^{flox/flox}*) mutant mice. In this study, *Auts2^{flox/flox}* mice were used as the controls. For the generation of *CaMKIIa-CreER^{T2};Auts2^{flox/flox}* mice, *CaMKIIa-CreER^{T2}* mice with mixed genetic background (F1: C57BL6N/FVB) were first crossed with *Auts2^{flox/flox}* mice (C57BL/6N background) to obtain *CaMKIIa-CreER^{T2};Auts2^{flox/+}* mice. *CaMKIIa-CreER^{T2};Auts2^{flox/+}* mice were then crossed with *Auts2^{flox/flox}* mice to obtain litters consisting of *Auts2^{flox/+}*, *Auts2^{flox/flox}*, *CaMKIIa-CreER^{T2};Auts2^{flox/+}* and *CaMKIIa-CreER^{T2};Auts2^{flox/flox}* mice. For all experiments, the *CaMKIIa-CreER^{T2};Auts2^{flox/flox}* males were crossed with *Auts2^{flox/flox}* females to yield the test animal cohorts consisting of the *CaMKIIa-CreER^{T2};Auts2^{flox/flox}* and *Auts2^{flox/flox}* littermates. All tested animals in the behavioral analyses were generated through at least 9 crosses with C57BL/6N background animals (e.g. *Auts2^{flox/flox}*) to obtain genetic backgrounds close to that of C57BL/6N. For the experiments with *CaMKIIa-CreER^{T2}* mice, tamoxifen (Sigma-Aldrich, St. Louis, MO, USA) was administered at 50 mg/kg during postnatal 21-25 days for anatomical analysis or P30-34 for behavioral analyses by intraperitoneal injection twice daily for 5 consecutive days and the analyses were performed at postnatal day 50 and 10-12 weeks, respectively. Mice were maintained in ventilated racks under a 12-h light/dark cycle with food and water ad libitum in temperature controlled, pathogen-free facilities. Mice of each genotype were randomly allocated to different experiments. Both male and female animals were used in anatomical and electrophysiological experiments. All animal experiments in this study have been approved by the Animal Care and Use Committee of the National Institute of Neuroscience, Japan, and the

guidelines established by the Institutional Animal Care and Use Committee of Nagoya University, the Guiding Principles for the Care and Use of Laboratory Animals approved by the Japanese Pharmacological Society, and the National Institutes of Health Guide for the Care and Use of Laboratory Animals. All efforts were made to minimize suffering and to reduce the number of animals used.

Behavioral analysis

For behavioral test battery using *Auts2^{delB}* mice, two independent cohorts of *Auts2^{delB/+}* heterozygotes and their wild type littermate male mice (8-19 weeks old) were tested, to confirm findings. All behavioral tests using *Auts2^{delB}* mice were obtained by crossing *Auts2^{delB/+}* heterozygous male mice with wild type C57BL6/N female mice (Charles River Laboratories, Kanagawa, Japan) to avoid the possibility that altered behaviors in the mutant dams could influence the postnatal development of their offspring. After weaning, male mice were cohoused in same-genotype groups of 2-4 littermates per cage before and during the behavioral tests.

Behavioral tests were performed using the same set of mice in the following sequence: locomotor activity, open field test, novel object recognition test, elevated plus maze, 3-chamber social interaction test, prepulse inhibition test, and fear conditioning test. For recording of USVs, buried food finding test, visual placing response test, thigmotaxis and reciprocal social interaction test, separate cohorts of mice were used.

For behavioral analyses using *CaMKIIa-CreER^{T2};Auts2^{flox}* conditional KO mice, *CaMKIIa-CreER^{T2};Auts2^{flox/flox}* homozygous mutant mice and their control littermate *Auts2^{flox/flox}* male mice were used.

The buried food finding test

The buried food finding test was carried out as described below (Yang and Crawley, 2009). Male mice were fasted for 18-24 hrs before testing. Subject mice were individually habituated in a clean cage (45 x 23 x 15 cm) for 5 min. For testing, a food pellet was buried at the end of the cage under 1 cm of wood-chip bedding. Subject mice were placed in the corner opposite to the site of the concealed food pellet. Movement of mice was recorded by video camera and time spent to explore the food pellet was measured by an examiner with stopwatch.

Visual placing response test

The function of the visual system was evaluated by the visual placing response according to the methods by Metz and Schwab (Metz and Schwab, 2004). In this test, the test mouse was suspended by its tail and lowered toward a solid object without any contact to the vibrissae. When the head of a mouse approaches near the edge of the object, the mouse normally raises its head and extends the forelimbs to place them onto the object. The procedure was conducted by three trials and the mean response was rated with the following scoring system: 0 indicates no observable placing behavior, 1 represents a weak or delayed placing response and 2 points indicates a clear placing reaction.

Whisker twitch reflex

The whisker twitch reflex was tested by approaching from behind and lightly touching one set of vibrissae, eliciting head turning to the side on which the vibrissae was touched (Miyakawa et al., 2001).

Thigmotaxis

Mice were placed in the center of the test chamber (26 cm x 26 cm x 40 cm) under moderately bright light conditions (100 lux) and allowed to explore it. Each 20 min session was monitored by video camera and analyzed in four 5 min bins. Time spent in the marginal area defined as a 4 cm band extending from the wall was measured by examiner with a stopwatch.

Locomotor activity

Spontaneous exploratory locomotion was examined as follows (Nagai et al., 2010). Mice were individually placed in a transparent acrylic cage with a black frosted Plexiglas floor (25×25×20 cm) under moderate light conditions (15 lux), and locomotor activity was measured every 5 min for 60 min using digital counters with an infrared sensor (BrainScience Idea, Osaka, Japan).

Open field test

Mice were placed in the center of the test chamber (diameter, 60 cm; height, 35 cm) under moderate light conditions (60 lux) and allowed to explore it for 5 min, while their activity was automatically analyzed using the ethovision automated tracking program (BrainScience Idea Co.

Ltd., Osaka, Japan) (Lee et al., 2005). The center zone of the open-field was defined as the 40 cm-diameter inner circle in the chamber. Movements were measured via a camera mounted above the open field. Measurements included distance traveled and time spent in the inner and outer sections.

Elevated-plus maze test

The apparatus consists of two open (25 × 8 × 0.5 cm), two closed (25 × 8 × 20 cm) arms and a common central zone (8 × 8 cm) to form a plus shape (Koike et al., 2009). The entire apparatus was elevated to 50 cm above floor level under moderately bright conditions (170 lux). The test begins by placing a mouse in the central zone of the maze facing an open arm. The animals were allowed to move freely in the maze for 5 min. An arm entry was defined as all four paws in the arm. The duration of time spent in an arm and number of arm entries is measured. Animal falling off open arms was excluded from analyses.

Reciprocal social interaction test

Reciprocal social interaction test was performed as described below (Harper et al., 2012; Hiramoto et al., 2011). Age-matched, non-littermate male WT and *Auts2*^{del8/+} mutant mouse pairs, or *CaMKIIa-CreER*^{T2};*Auts2*^{fllox/fllox} and *Auts2*^{fllox/fllox} control mice pairs were tested. Each individual mouse was placed in a new cage in the experimental room for 30 min. Pairs of unfamiliar mice (non-cage mate and non-littermate) with age-matched, same genotype were then placed in a new, third cage (45 x 23 x 15 cm) for two 5 min sessions with a 30 min interval. Behaviors were monitored with video camera and time spent in active behaviors were analyzed by examiner with a stopwatch. Active social behaviors included aggressive forms (i.e. wrestling, boxing, kicks, mounting, tail rattle, bites, sideway offense and pursuit) and affiliative forms (i.e. olfactory investigation and allogrooming).

Three-chamber social interaction test

A three-chamber arena was used to examine social approach and preference for social novelty as follows (Nadler et al., 2004). During habituation, empty cylinders were placed in each end chamber. The test subject was placed in the center chamber and its behavioral approach to the chambers was monitored for 10 min. During the sociability test, an unfamiliar male C57BL/6N

mouse (stranger 1) that had no prior contact with the test mouse was put in one of the empty chambers, and the behavioral approach to the empty chamber and stranger 1 was monitored for 10 min. During the social novelty test, new unfamiliar male C57BL/6N mouse (stranger 2) was placed in another chamber, and the behavioral approach to the stranger 1 and stranger 2 was monitored for additional 10 min. The amount of time spent in each arena was measured by an ethovision automated tracking program (Noldus, Wageningen, Netherlands).

Novel object recognition test

A novel object recognition test was carried out as described below (Nagai et al., 2007). Mice were individually habituated to an open box (30 × 30 × 35 cm) for 3 days. All sessions were performed under conditions of illumination (16 lux). During the training session, two novel objects of similar size were placed in the open box and mice were allowed to explore for 10 min. The objects were a golf ball, wooden cylinder, and square pyramid, which were different in shape and color. An animal was considered to be exploring the object when its head was facing the object or it was touching or sniffing the object. The time spent exploring each object was recorded by using video camera and analyzed in a double-blind manner. During retention sessions, mice were placed back into the same box 24 h after the training session, one of the familiar objects used during training session was replaced by a novel object, and the mice were allowed to explore the two objects freely for 5 min. The exploratory index in the retention session, the ratio of the amount of time spent exploring the novel object to the total time spent exploring both objects, was used to measure cognitive function. In the training session, the preference index was calculated as the ratio of time spent exploring the object that was replaced by a novel object in the retention session to the total exploration time.

Cued and contextual fear conditioning test

Cued and contextual fear conditioning test was carried out as described below (Ibi et al., 2010). Training took place in the chamber (30 × 30 × 40 cm) equipped with a metal floor and a 15-sec white noise tone (85 dB) was delivered (conditioned stimulus). During the last 5 sec of the tone stimulus, a foot shock of 0.8 mA was delivered through a shock generator as an unconditioned stimulus (Brainscience Idea Co. Ltd., Osaka, Japan). This procedure was repeated four times at 15-sec intervals. Twenty-four hr after conditioning, the context-dependent test was

performed. For the context-dependent test, each mouse was put in the training chamber, and the freezing response was monitored for 2 min in the absence of the conditioned stimulus. Tone-dependent testing was performed 4 hr after the context-dependent test. For the tone-dependent test, the freezing response was measured for 1 min in a standard transparent rectangular rodent cage (25 × 30 × 18 cm) in the presence of a continuous-tone stimulus identical to the conditioned stimulus using mice that had been subjected to the context-dependent test.

Prepulse inhibition (PPI) test

The PPI test was carried out as follows (Takahashi et al., 2007). The animals were placed in the chamber (San Diego Instruments, San Diego, California) and were habituated for 10 min. During the habituation time, 65 dB background white noise was delivered. Mice then received 10 startle trials, 10 no-stimulus trials and 40 PPI trials. The intertrial stimulus intervals were between 10 and 20 sec and the total session lasted 17 min. Mice were presented with a single 120 dB white noise burst lasting 40 msec during the startle trial. PPI trials consisted of a prepulse (20 msec burst of white noise at 69, 73, 77 or 81 dB intensity) followed, 100 msec later, by the startle stimulus (120 dB, 40 msec white noise). Each of the four prepulse trials (69, 73, 77 or 81 dB) was performed 10 times. Sixty different trials were pseudo-randomly delivered, ensuring that each trial was carried out 10 times and that no two consecutive trials were identical. The resulting movement of the animal in the startle chamber was measured for 100 msec after startle stimulus onset (sampling frequency 1 kHz), rectified, amplified and fed into a computer, which calculated the maximal response over the 100 msec. Basal startle amplitude was determined as the mean amplitude of the 10 startle trials. PPI was calculated according to the following formula: $100 \times [1 - (PPx/P120)] \%$, in which PPx is the mean amplitude of the 10 PPI trials (PP69, PP73, PP75 or PP80) and P120 is the basal startle amplitude.

Ultrasonic vocalizations

Ultrasonic Vocalizations were recorded using an UltraSoundGate system (Avisoft bioacoustics, Glienicke, Germany) composed of a CM16/CMPA condenser microphone, Avisoft-UltraSoundGate 116H computer interface, and Avisoft Recorder software with a sampling rate of 400 kHz. A microphone was hung 16 cm above the floor of a sound attenuating chamber. For

the test, male mice were individually housed in Plexiglas cages (23 cm x 16 cm x 12 cm) for a week prior to test time to acclimate to the testing environment. Unfamiliar wild type three month old C57BL6/N female mice were placed into the test male cage and recordings begun after USV was detected and continued for 1 min period.

Syllable analysis

Vocal signals recorded in wav files were automatically detected by MATLAB-based software USVSEG with modification to mouse USVs (Tachibana et al., 2014). This software segments each syllable and exports as individual jpeg files. As Tachibana et al reported (Tachibana et al., 2020), USVSEG can detect correct vocal signals with approximately 95% accuracies compared to the information that was manually defined by a human examiner. The number of USVs and duration of each call are automatically detected. By observing jpeg files, experimenters then manually excluded the files of vocalizations that includes only click-like sounds without any tone-like signals or that could not be classified into any of the call types as noises (false positive).

The vocalizations were manually categorized into 12 types observing these jpeg files based on the previously published criteria with some modification (Kikusui et al., 2011; Yasumura et al., 2014). In the previous criteria, syllables including both jumps and harmonics were classified into One Jump or More jump. In our present methods, such syllables were classified in more detailed manner in order to demonstrate more clearly whether such Jumps include harmonics or not. In addition, these 12 call types were grouped into "simple" and "complicated" syllable types based on call duration, frequency modulation and the presence/absence of harmonics or jumps. The call classifications we used are as follows;

Upward. Syllables with upwardly modulated frequency change (> 5 kHz)

Downward. Syllables with downwardly modulated frequency change (> 5 kHz).

Flat. Syllables with few frequency modification \leq 5 kHz.

Short. syllables which is shorter than or equal to 5 msec.

Chevron. Syllables with an upsweep (greater than 5 kHz) followed by a down-sweep (greater than half of the frequency change of the upsweep) or reversed one, formed like a U or a reversed U.

Wave. Syllables with two directional changes in frequency (> 5 kHz).

Complex. Syllables with three or more directional changes in frequency (> 5 kHz).

One jump. Syllables with one frequency jump and no time gap before and after jump.

More jump. Syllables with two or more frequency jumps and no time gap before and after jumps.

Harmonics. syllables that were displayed as one main component stacking with other harmonically components of different frequency (without jumps).

One jump + harmonics. Syllables with components of both One jump and Harmonics.

More jump + harmonics. Syllables with components of both More jump and Harmonics.

Plasmid construction

The plasmid construction of pCAG-Myc-AUTS2-full length, FL-AUTS2^R (the shRNA-resistant AUTS2-full length), NES-FL-AUTS2^R and S-AUTS2-var.2 were described previously (Hori et al., 2014). cDNA fragments for S-AUTS2-var.1 encoding 1,372-3,786 bp were amplified by PCR using full-length *Auts2* cDNA as a template and subcloned into pCAGGS vector. To construct the 3xNLS-AUTS2 expression plasmid, two oligonucleotides coding the three tandem nuclear localization signal (NLS) sequence of the SV40 Large T-antigen (PKKKRKV) were annealed and inserted between Myc-tag and 5'-terminus of AUTS2 ORF in pCAG-Myc-AUTS2^R with EcoRI site: Fwd, (5'-AATTGGTGCACGTGGATCCAAAAAAGAAGAGAAAGGTAGATCCAAAAAAGAAGAGAAAGGTAGATCCAAAAAAGAAGAGAAAGGTACACGTGTCCG-3'): Rev, (5'-AATTCGGACACGTGTACCTTTCTCTTCTTTTTGGATCTACCTTTCTCTTCTTTTTGGATCTACCTTTCTCTTCTTTTTGGATCCACGTGCACC-3'). The expression plasmids for EGFP, Cre recombinase and shRNAs were described previously (Hori et al., 2014).

Primary culture of hippocampal neurons

Primary hippocampal cultures were prepared as described below (Hori et al., 2014; Hori et al., 2005). Hippocampi at E17.5 were dissected from C57BL6/N wild type or homozygotic *Auts2*^{flox/flox} mouse embryos and dissociated using Neuron Dissociation Solution S (Fujifilm Wako Pure Chemical Corporation, Osaka, Japan). The dispersed neurons were electroporated with the expression plasmids or shRNA vectors using the NEPA21 electroporator (Nepa Gene, Chiba, Japan) according to the manufacturer's instructions. The electroporated neurons were mixed with the transfection-free control neurons at a ratio of approximately 1:20 and plated on coverslips coated with 0.1 mg/ml poly-D-lysine (Sigma-Aldrich, St. Louis, MO, USA) at a density

of 8,000 – 12,000 cells/cm² and maintained in astroglial-conditioned Neurobasal medium containing 2% B27 supplement (Thermo Fisher Scientific, Waltham, MA, USA) and 1 mM L-glutamine.

Immunostaining

For immunocytochemistry, cells were fixed with 4% PFA / 4% sucrose for 40 min on ice. Immunostaining was performed using the following primary antibodies: mouse anti-PSD-95 (6G6-1C9, ThermoFisher Scientific, Waltham, MA, USA), mouse anti-Gephyrin (3B11, Synaptic Systems, Goettingen, Germany), rabbit anti-Synapsin-1 (D12G5, Cell Signaling Technology, MA, USA), rat anti-GFP (RQ1, gift from A. Imura, BRI, Kobe), mouse anti-Myc-tag (M192-3, MBL, Nagoya, Japan). For immunohistochemistry, adult mouse brains were dissected after mice were deeply anesthetized and transcardially perfused with 4% PFA. The brains were post-fixed with 4% PFA / 5% sucrose for 6 hrs or overnight at 4 °C, rinsed with PBS, cryoprotected with 30% sucrose, embedded in O.C.T compound (Sakura Fine-Tek, Tokyo, Japan), and cryosectioned at 14~30 µm. For presynaptic marker staining, tissue sections were blocked with 5% normal donkey serum / 1% BSA and 0.1% Triton X100 in PBS and immunolabeled with guinea pig anti-VGLUT1 (AB5905, Merck Millipore, Burlington, MA, USA) and rabbit anti-VGAT (AB5062P, Merck Millipore, Burlington, MA, USA) antibodies overnight at 4 °C. For quantification of presynaptic puncta number, fluorescence images of mPFC regions were acquired using 100x objective equipped with a confocal laser scanning microscope FV1000 (Olympus, Tokyo, Japan), magnified three fold and analyzed using the “analyze particle” module in Fiji-imageJ software (Schindelin et al., 2012).

For c-Fos staining, tissue sections were immunostained with rabbit anti-c-Fos antibody (sc-52, Santa Cruz Biotechnology, Inc., Dallas, TX, USA). Acquisition of fluorescent images, counts and measurement of dendritic protrusions were carried out using a Zeiss LSM 780 confocal microscope system and ZEN software (Carl Zeiss, Oberkochen, Germany). For analysis of dendritic arbors, images were acquired using a Plan-Apochromat 20×/0.8 differential interference contrast (DIC) objective. Tracing, measurement of dendritic length and Sholl analysis were performed using NeuroLucida software (MBF Bioscience, Williston, VT, USA). For analysis of dendritic spines, compiled z-stack images were acquired using a Plan-Apochromat 63×/1.40 oil-immersion DIC objective at 0.37 µm intervals, sampling above and below the

dendrites. Maximum intensity projections were used for quantification. For DAB staining with rat anti-GFP antibody (RQ1), the sections were processed using the VECTASTAIN ABC system (Vector Laboratories, Burlingame, CA, USA) with diaminobenzidine (Sigma-Aldrich, St. Louis, MO, USA) and images were taken on Keyence All-in-One fluorescence microscope (BZ-X700, Osaka, Japan).

Immunoblotting

The lysates of HEK293T cells transfected with AUTS2 expression plasmids or cerebral cortices from mouse brain at P0 were solubilized in SDS sample buffer and separated in 2-15% gradient gel by SDS-PAGE (Gellex International co.ltd., Tokyo, Japan). Proteins transferred onto a PVDF membrane were immunoblotted with anti-AUTS2 antibody (HPA000390, Sigma-Aldrich, St. Louis, MO, USA) and anti-GAPDH (2118S, Cell Signaling Technology, Tokyo, Japan) antibodies, and visualized using HRP-conjugated secondary antibody (GE Healthcare, Chicago, IL, USA) followed by ECL Prime (GE Healthcare, Chicago, IL, USA). Signals were detected with a cooled CCD camera (LAS-4000 mini; Fujifilm, Kanagawa, Japan).

Golgi-staining

Whole brains collected from mice were subjected to Golgi impregnation solution (FD Rapid GolgiStain kit, FD NeuroTechnologies, Columbia MD, USA). Coronal sections with 80-100 μm thick were obtained with cryostat and mounted on gelatin-coated slides. After tissues were processed for Golgi-Cox staining according to manufacturer's instructions, the brain sections were dehydrated with a graded series of ethanol, immersed in xylene, and embedded in Entellan (Merck, Darmstadt, Germany). Neurons were traced under bright-field using a Leica microscope (DM5000B, Leica Microsystems, Danaher, Germany) with a 100x oil-immersion objective and were 3D-reconstructed by Neurolucida Software.

Spine measurements

For primary cultured neurons, spines or synaptic puncta immuno-labeled with synapse markers along secondary dendritic segments randomly selected ($>30 \mu\text{m}$ length) were counted. For Golgi-stained tissue samples, spines along primary apical dendrites immediately proximal to the cell soma (0 – 50 μm) of cortical layer II/III and CA1 hippocampal pyramidal neurons, or

spines along secondary dendrites within 100 μm from the soma of the neurons indicated in the figure were examined. Spine densities were calculated as mean number of spines per 10 μm dendrites. On the basis of spine morphology, dendritic protrusions were classified into the following four categories (Harris and Kater, 1994): thin (≥ 0.5 μm protrusions with small bulbous head less than twice as large as spine neck), mushroom (≥ 0.5 μm protrusions with bulbous head more than twice as large as spine neck), stubby (≥ 0.5 μm protrusions with bulbous head but without a neck), filopodia (≥ 5 μm long and thin protrusions without bulbous heads). Dendritic protrusions with total lengths exceeding 10 μm were considered as branched dendrites and excluded from the analysis. Z-stack images of dendritic spines were taken using a Keyence All-in-One microscope with a 40x objective (BZ-X700, Osaka, Japan).

Electrophysiology

Whole-cell voltage-clamp recordings of mEPSCs and mIPSCs using brain slices were conducted as follows (Takahashi et al., 2012). Coronal hippocampal slices with 400 μm thickness from adult mice at P33-44 were prepared in ice-cold dissection buffer (300 mM sucrose, 3.4 mM KCl, 0.6 mM NaH_2PO_4 , 10 mM D-Glucose, 10 mM HEPES, 3.0 mM MgCl_2 , 0.3 mM CaCl_2 at pH 7.4) using a VT1200S vibratome (Leica Biosystems, Danaher, Germany). Hippocampal slices were incubated in artificial cerebrospinal fluid (ACSF; 119 mM NaCl, 2.5 mM KCl, 1.0 mM NaH_2PO_4 , 26.2 mM NaHCO_3 , 11 mM D-Glucose, 4.0 mM MgSO_4 , 4.0 mM CaCl_2 , gassed with 95% O_2 and 5% CO_2), left to recover for more than 1 hour at room temperature, and then transferred to a recording chamber mounted on an upright microscope (BX61WI, Olympus, Tokyo, Japan). For voltage-clamp recordings of hippocampal slices, borosilicate glass pipettes (4-6 $\text{M}\Omega$) were filled with the internal solutions (135 mM CsMeSO_4 , 10 mM HEPES, 0.2 mM EGTA, 8 mM NaCl, 4 mM Mg-ATP, 0.3 mM Na_3GTP at pH 7.2, osmolality adjusted to 280-300 mOsm). All data of whole-cell voltage-clamp recordings were acquired with Multiclamp 700B (Molecular Devices, San Jose, CA, USA) equipped with an A/D converter (BNC-2090, National Instruments, Austin, TX, USA or Digidata 1550B, Molecular Devices) and Igor Pro software version 4.01 (Wavemetrics, Portland, OR, USA) or pClamp 10 software (Molecular Devices) at 4 kHz. Series resistances were monitored, and the data were discarded when the series resistance changed by > 30 $\text{M}\Omega$ during recordings. mEPSCs were recorded at -70 mV in the presence of 1 μM tetrodotoxin and 100 μM picrotoxin, and mIPSCs were recorded at 0 mV in the presence of 1 μM tetrodotoxin, 10 μM

CNQX and 50 μ M D-APV. mEPSCs and mIPSCs events above a threshold value (10 pA) were analyzed with MiniAnalysis software version 6.0.3 (Synaptosoft, Fort Lee, NJ, USA). For measurement of paired-pulse EPSCs, a bipolar stimulating electrode (FHC, Bowdoin, ME, USA) was placed in the stratum radiatum to stimulate Schaffer collaterals pathway. Pairs of evoked-EPSCs were recorded at a holding potential of -70 mV in the presence of 100 μ M picrotoxin in the bath solution, and 2 mM QX-314 was added in internal solution. The pulse intensity was adjusted to 30–50% of the maximum amplitude. The stimulus frequency was 0.1 Hz. Inter-stimulus intervals of paired-pulse stimuli were set at 50 ms, 250 ms, 500 ms and 1000 ms.

qPCR

Total RNA was purified using the Qiagen RNeasy Plus Universal mini kit (QIAGEN, Hilden, Germany). Purified total RNA (0.5 μ g) was subsequently reverse transcribed to cDNA using the ReverTra Ace qPCR RT kit (Toyobo, Osaka, Japan) according to the manufacturer's instructions. Real-time qPCR was performed with PowerUp SYBR Green Master Mix (Thermo Fisher Scientific, Waltham, MA, USA) in an applied Biosystems 7300 Real Time PCR System and relative expression was calculated via the 2Δ method and results were normalized to the internal control β -actin. The primers (sense and antisense, respectively) were as follows: mouse *Auts2*, 5'-AGAGCCTCTCACAGCCACTG-3' and 5'-GGTGGTGGGAGATGTGAGGA-3'; β -actin, 5'-GGCTGTATTCCCCTCCATCG-3', and 5'-CCAGTTGGTAACAATGCCATGT-3'.

RNA-sequencing and data analysis

Total RNA was extracted from hippocampal tissues of 4 control (*Auts2^{flox/flox}*) and 4 KO (*Emx1^{Cre/+};Auts2^{flox/flox}*) mice at P14 using RNeasy Plus Universal Kit (QIAGEN, Hilden, Germany). Quality analyses and quantification of extracted RNA were performed using NanoDrop and Qubit Fluorometer (Thermo Fisher Scientific, Waltham, MA, USA), respectively. Sequencing libraries were prepared using the NEBNext Ultra Directional RNA Library Prep Kit for directional libraries (New England BioLabs, Tokyo, Japan) and the KAPA HTP Library Preparation Kits (KAPA Biosystems, Wilmington, MA, USA) according to the manufacturer's instructions. The RNA-seq libraries were sequenced (101 cycles) using the Illumina HiSeq platforms.

Raw sequence reads were aligned to the reference mouse genomes (GRCm38/mm10) by HISAT2 (Kim et al., 2015). Genome-wide expression levels were measured as a unit of transcripts

per kilobase million (TPM) using StringTie(Pertea et al., 2015) and the numbers of reads were counted per gene per sample using htseq-count within HTSeq (Anders et al., 2015). Finally, differentially expressed genes (DEGs) were identified by DESeq2 (Love et al., 2014). For gene ontology analysis, DAVID bioinformatics Resources 6.8 was used (National Institute of Allergy and Infectious Diseases-National Institute of Health; <https://david.ncifcrf.gov>). RNA-seq data has been deposited into GEO database with the accession number GSE134712.

Sample size and statistical analysis

Sample size was determined based on studies using established methods and on our previous experiments (Hori et al., 2015; Hori et al., 2014; Hori et al., 2005; Takahashi et al., 2012). Data analyses were performed blinded to the genotype. The number of samples and animals is indicated in the figure legends. All statistical analyses except transcriptome data processing and analysis were performed using GraphPad Prism 7 (GraphPad Software, La Jolla CA, USA). The normal distribution of data was confirmed by the Shapiro-Wilks test and if significant, a nonparametric Mann Whitney U test was used for comparison. Equal variance was tested by the F-test and when there was a significant difference, we used a two-tailed unpaired t-test with Welch's correction. When the data were within the assumptions of normal distribution and equal variance, a two-tailed unpaired t-test was used for comparison of the means between two groups. For comparison of more than 2 groups, a one-way analysis of variance (ANOVA) followed by the Dunnett's multiple comparison test was used.

In the behavioral analysis, two-way ANOVA followed by the Bonferroni test was used for multiple-group comparisons (reciprocal social interaction test and three-chamber social interaction test). Two-way ANOVA with repeated measurements followed by the Bonferroni test was used for multiple-group comparisons (locomotor activity, novel object recognition test, thigmotaxis and prepulse inhibition test).

Supplemental References

Anders, S., Pyl, P.T., and Huber, W. (2015). HTSeq--a Python framework to work with high-throughput sequencing data. *Bioinformatics* 31, 166-169.

Erdmann, G., Schutz, G., and Berger, S. (2007). Inducible gene inactivation in neurons of the adult mouse forebrain. *BMC Neurosci* 8, 63.

Harper, K.M., Hiramoto, T., Tanigaki, K., Kang, G., Suzuki, G., Trimble, W., and Hiroi, N. (2012). Alterations of social interaction through genetic and environmental manipulation of the 22q11.2 gene *Sept5* in the mouse brain. *Hum Mol Genet* 21, 3489-3499.

Harris, K.M., and Kater, S.B. (1994). Dendritic spines: cellular specializations imparting both stability and flexibility to synaptic function. *Annu Rev Neurosci* 17, 341-371.

Hiramoto, T., Kang, G., Suzuki, G., Satoh, Y., Kucherlapati, R., Watanabe, Y., and Hiroi, N. (2011). *Tbx1*: identification of a 22q11.2 gene as a risk factor for autism spectrum disorder in a mouse model. *Hum Mol Genet* 20, 4775-4785.

Hori, K., Nagai, T., Shan, W., Sakamoto, A., Abe, M., Yamazaki, M., Sakimura, K., Yamada, K., and Hoshino, M. (2015). Heterozygous Disruption of Autism susceptibility candidate 2 Causes Impaired Emotional Control and Cognitive Memory. *PLoS One* 10, e0145979.

Hori, K., Nagai, T., Shan, W., Sakamoto, A., Taya, S., Hashimoto, R., Hayashi, T., Abe, M., Yamazaki, M., Nakao, K., *et al.* (2014). Cytoskeletal regulation by *AUTS2* in neuronal migration and neuritogenesis. *Cell reports* 9, 2166-2179.

Hori, K., Yasuda, H., Konno, D., Maruoka, H., Tsumoto, T., and Sobue, K. (2005). NMDA receptor-dependent synaptic translocation of insulin receptor substrate p53 via protein kinase C signaling. *J Neurosci* 25, 2670-2681.

Ibi, D., Nagai, T., Koike, H., Kitahara, Y., Mizoguchi, H., Niwa, M., Jaaro-Peled, H., Nitta, A., Yoneda, Y., Nabeshima, T., *et al.* (2010). Combined effect of neonatal immune activation and mutant *DISC1* on phenotypic changes in adulthood. *Behav Brain Res* 206, 32-37.

Iwasato, T., Datwani, A., Wolf, A.M., Nishiyama, H., Taguchi, Y., Tonegawa, S., Knopfel, T., Erzurumlu, R.S., and Itohara, S. (2000). Cortex-restricted disruption of *NMDAR1* impairs neuronal patterns in the barrel cortex. *Nature* 406, 726-731.

Kikusui, T., Nakanishi, K., Nakagawa, R., Nagasawa, M., Mogi, K., and Okanoya, K. (2011). Cross fostering experiments suggest that mice songs are innate. *PLoS One* 6, e17721.

Kim, D., Langmead, B., and Salzberg, S.L. (2015). HISAT: a fast spliced aligner with low memory requirements. *Nature methods* 12, 357-360.

Koike, H., Ibi, D., Mizoguchi, H., Nagai, T., Nitta, A., Takuma, K., Nabeshima, T., Yoneda, Y., and Yamada, K. (2009). Behavioral abnormality and pharmacologic response in social isolation-reared mice. *Behav Brain Res* 202, 114-121.

Lee, P.R., Brady, D.L., Shapiro, R.A., Dorsa, D.M., and Koenig, J.I. (2005). Social interaction

deficits caused by chronic phencyclidine administration are reversed by oxytocin. *Neuropsychopharmacology* 30, 1883-1894.

Love, M.I., Huber, W., and Anders, S. (2014). Moderated estimation of fold change and dispersion for RNA-seq data with DESeq2. *Genome Biol* 15, 550.

Metz, G.A., and Schwab, M.E. (2004). Behavioral characterization in a comprehensive mouse test battery reveals motor and sensory impairments in growth-associated protein-43 null mutant mice. *Neuroscience* 129, 563-574.

Miyakawa, T., Yared, E., Pak, J.H., Huang, F.L., Huang, K.P., and Crawley, J.N. (2001). Neurogranin null mutant mice display performance deficits on spatial learning tasks with anxiety related components. *Hippocampus* 11, 763-775.

Nadler, J.J., Moy, S.S., Dold, G., Trang, D., Simmons, N., Perez, A., Young, N.B., Barbaro, R.P., Piven, J., Magnuson, T.R., et al. (2004). Automated apparatus for quantitation of social approach behaviors in mice. *Genes, brain, and behavior* 3, 303-314.

Nagai, T., Kitahara, Y., Shiraki, A., Hikita, T., Taya, S., Kaibuchi, K., and Yamada, K. (2010). Dysfunction of dopamine release in the prefrontal cortex of dysbindin deficient sandy mice: an in vivo microdialysis study. *Neurosci Lett* 470, 134-138.

Nagai, T., Takuma, K., Kamei, H., Ito, Y., Nakamichi, N., Ibi, D., Nakanishi, Y., Murai, M., Mizoguchi, H., Nabeshima, T., et al. (2007). Dopamine D1 receptors regulate protein synthesis-dependent long-term recognition memory via extracellular signal-regulated kinase 1/2 in the prefrontal cortex. *Learn Mem* 14, 117-125.

Pertea, M., Pertea, G.M., Antonescu, C.M., Chang, T.C., Mendell, J.T., and Salzberg, S.L. (2015). StringTie enables improved reconstruction of a transcriptome from RNA-seq reads. *Nat Biotechnol* 33, 290-295.

Schindelin, J., Arganda-Carreras, I., Frise, E., Kaynig, V., Longair, M., Pietzsch, T., Preibisch, S., Rueden, C., Saalfeld, S., Schmid, B., et al. (2012). Fiji: an open-source platform for biological-image analysis. *Nature methods* 9, 676-682.

Tachibana, R.O., Kanno, K., Okabe, S., Kobayasi, K.I., and Okanoya, K. (2020). USVSEG: A robust method for segmentation of ultrasonic vocalizations in rodents. *PLoS One* 15, e0228907.

Tachibana, R.O., Oosugi, N., and Okanoya, K. (2014). Semi-automatic classification of birdsong elements using a linear support vector machine. *PLoS One* 9, e92584.

Takahashi, H., Katayama, K., Sohya, K., Miyamoto, H., Prasad, T., Matsumoto, Y., Ota, M., Yasuda, H., Tsumoto, T., Aruga, J., et al. (2012). Selective control of inhibitory synapse development by Slitrk3-PTPdelta trans-synaptic interaction. *Nat Neurosci* 15, 389-398, S381-382.

Takahashi, K., Nagai, T., Kamei, H., Maeda, K., Matsuya, T., Arai, S., Mizoguchi, H., Yoneda, Y., Nabeshima, T., Takuma, K., et al. (2007). Neural circuits containing pallidotegmental GABAergic neurons are involved in the prepulse inhibition of the startle reflex in mice. *Biol Psychiatry* 62,

148-157.

Yang, M., and Crawley, J.N. (2009). Simple behavioral assessment of mouse olfaction. *Curr Protoc Neurosci Chapter 8, Unit 8 24*.

Yasumura, M., Yoshida, T., Yamazaki, M., Abe, M., Natsume, R., Kanno, K., Uemura, T., Takao, K., Sakimura, K., Kikusui, T., *et al.* (2014). IL1RAPL1 knockout mice show spine density decrease, learning deficiency, hyperactivity and reduced anxiety-like behaviours. *Sci Rep 4, 6613*.